CD105+ fibroblasts support an immunosuppressive niche in women at high risk of breast cancer initiation

Eric G. Carlson
City of Hope
Jennifer C. Lopez
City of Hope
Yukiko Yamaguchi
City of Hope
Jackson Gibson
City of Hope
Saul Priceman
City of Hope
Mark A. LaBarge
mlabarge@coh.org
City of Hope

Research Article

Keywords: Intralobular fibroblasts, aging, BRCA1, macrophages, immunosuppressive

Posted Date: April 2nd, 2025

DOI: https://doi.org/10.21203/rs.3.rs-5777126/v1

Additional Declarations: No competing interests reported.

Abstract

Background:

Aging is the greatest risk factor for breast cancer, and although epithelial cells are the source of carcinomas, epithelial changes alone do not fully explain cancer susceptibility. Fibroblasts and macrophages are key stromal constituents around the cells of origin for cancer in breast tissue. With age, macrophages surrounding terminal ductal lobular units (TDLUs) become increasingly immunosuppressive. $CD105^{+}$ fibroblasts intercalate within TDLUs, drive luminal differentiation, and give rise to immunosuppressive cancer-associated fibroblasts in other tissues. We propose that differences in fibroblasts are a crucial component of the stroma that shapes cancer susceptibility.

Methods:

Primary fibroblast cultures were established from prophylactic and reduction mammoplasties from women ranging in age from 16 to 70 years and breast cancer risk (*BRCA1* mutation carriers). Growth characteristics, transcriptional profiles, differentiation potential, and secreted proteins were profiled for fibroblast subtypes from diverse donors. Co-cultures with fibroblasts, monocytes, macrophages, and T cells were used to ascertain the functional role played by $CD105^{+}$ fibroblasts in immune cell modulation.

Results:

We found that peri-epithelial $CD105^{+}$ fibroblasts are enriched in older women as well as women who carry *BRCA1* mutations. These $CD105^{+}$ fibroblasts exhibit robust adipogenesis and secrete factors related to macrophage polarization. Macrophages cocultured with fibroblasts better maintain or enhance polarization states than media alone. $CD105^{+}$ fibroblasts increased expression of immunosuppressive macrophage genes. $CD105^{+}$ fibroblasts supported anti-inflammatory macrophage-mediated suppression of T cell proliferation, whereas $CD105^{-}$ fibroblasts significantly reduced the suppressive effect of anti-inflammatory macrophages on T cell proliferation.

Conclusions:

Establishment of a coculture system to dissect the molecular circuits between $CD105^{+}$ fibroblasts and macrophages that drive immunosuppressive macrophage polarization has broad utility in understanding mammary gland development and events that precede cancer initiation. $CD105^{+}$ fibroblasts and macrophages may coordinate to suppress immunosurveillance and increase breast cancer susceptibility.

Background

The epithelial structures within the breast responsible for producing milk during lactation are known as terminal ductal lobular units (TDLUs). A TDLU is a collection of acini arising from one terminal duct and is embedded in intralobular stroma, which all together, is considered a functional unit of the breast. These structures are incredibly dynamic and are characterized by extracellular matrix (ECM) and cellular turnover throughout a woman's life (1–4). It is within these highly dynamic structures that breast cancer arises (5, 6).

Understanding how the dynamic microenvironment of the breast contributes to increased susceptibility of breast cancer initiation would improve risk stratification of women and open opportunities for the development of preventative therapeutics. Essential components of the intralobular stroma are fibroblasts and macrophages. The type-1 transmembrane glycoprotein endoglin (CD105, *ENG*) and dipeptidyl peptidase-4 (CD26, *DPP4*) are expressed by fibroblast subpopulations in healthy and diseased breast tissue (7–10). CD26 has been used as a marker for fibroblast subtypes in the mouse mammary gland (11, 12), whereas it is unstable in culture and has weaker protein-level expression when compared to CD105 in humans (8, 13–15). Fibroblasts that express CD105 ($CD105^+$) describe a population that is enriched in the intralobular stroma (8). Macrophages play essential roles in mammary gland homeostasis and development (16–18).They also defend against pathogens, are plastic, and may be categorized according to different functions. Classically activated, or pro-inflammatory, macrophages migrate to inflamed tissues, kill pathogens through the production of reactive oxygen species, and are capable of activating the adaptive immune system (19). Alternatively activated, or anti-inflammatory, macrophages facilitate tissue repair and induce immune tolerance by attracting regulatory T cells (Tregs) and Th2 T cells devoid of cytotoxic function (20). Postmenopausal women have more anti-inflammatory macrophages in their breasts compared to premenopausal women (21) and these anti-inflammatory macrophages preferentially localize to intralobular stroma when compared to their pro-inflammatory counterparts (22). How proportions of fibroblast subtypes change with age and breast cancer risk is an emerging area of interest in understanding cancer susceptibility (23, 24). Additionally, while interactions between fibroblasts and macrophages are well studied in tumor microenvironments (25–28), how these interactions in normal tissue contribute to breast cancer susceptibility is not well understood.

Herein, peri-epithelial fibroblast subtype composition was defined in early passage, finite fibroblast strains from 30 different women to evaluate how fibroblasts change in average risk older women and high-risk women with pathogenic *BRCA1* mutations. Numerous assays were performed to determine differences between $CD105^+$ and $CD105^-$ fibroblasts from different individuals at the transcriptional, protein, and functional levels. Immune cell cocultures were established between fibroblast subtypes and innate and adaptive immune cells. The signature for primary $CD105^+$ fibroblasts in culture was applied to publicly available human breast atlas datasets to ground the relevance of the findings *in vivo*. $CD105^+$ fibroblasts were found to be enriched in cultures established from women at high risk of developing breast cancer, were enriched for pathways related to an inflammatory milieu with the potential for

negative regulation of the immune system, exhibited robust adipogenic potential, and were found to influence macrophage polarization both in culture and *in vivo*.

Methods

Human subjects

The present study was approved by the Human Subjects Committee and the Institutional Review Board (IRB) 17185 at City of Hope. Twenty-five women were consented in person and sequentially; all women signed a City of Hope IRB-approved consent before trial entry. Women were eligible for the present study if they were undergoing a breast reduction or prophylactic mastectomy. Ten breast organoids from reduction mammoplasties were used to establish fibroblast strains prepared at the Lawrence Berkeley National Laboratory (Berkeley, CA) with approved IRB for sample distribution and collection from specific locations. Metadata including: age, BMI, self-reported ethnicity, family history of cancer, treatment, diagnosis, and *BRCA1* mutational status are included in **Supplementary Table 1**. Three leukapheresis products (whole blood discard kits) were obtained from consented healthy donors under protocols approved by the City of Hope Internal Review Board.

Isolation of fibroblasts

Peri-epithelial fibroblasts were isolated from primary organoids using differential trypsinization, as described previously (29). Briefly, Human mammary tissue is obtained as discard material from surgical procedures. The epithelial areas are separated from the stromal matrix of adipose tissue, connective tissue, and blood vessels using sterile scalpels. The epithelial tissue is cut into smaller 3–4 mm pieces to aid digestion. The dissected epithelial tissue is placed in a conical centrifuge tube and enzymatically digested in media supplemented with 200 U/ml crude collagenase and 100 U/ml hyaluronidase overnight at 37°C with gentle agitation. The tube is centrifuged to discard supernatant fat and medium. Organoids are resuspended in media. Digestion is complete when microscopic examination of organoids shows presence of ductal, alveolar, or ductal-alveolar structures. Digested organoids are added to a 100 µm cell strainer over a sterile 50 ml tube. Organoids are washed and the organoids that do not pass through the filter are collected and plated (approximately 20–40 organoids seeded per 60 mm dish). Cell migration from the organoids is visible by 24–48 hours, and mitotic outgrowth by 48–72 hours. Differential trypsinization with 0.05% trypsin is used to isolate the peri-epithelial fibroblasts from the outgrowths based on the rapid detachment of fibroblasts from the surface plastic, relative to epithelial cells. The peri-epithelial fibroblasts are collected and frozen for future expansion. Fibroblasts were maintained on 100mm culture dishes (Greiner Cellstar) in M87A medium (30) supplemented with 5% FBS (Gemini Bio-Products). To ensure that changes to CD105 expression were not cell culture artifacts, fibroblasts were maintained at subconfluence and dissociated with 0.05% trypsin for less than 5 minutes for passaging. 0.05% trypsin was found to produce identical CD105 expression patterns as a non-

enzymatic dissociation method, 1mM EDTA. Each strain was confirmed to be negative for mycoplasma prior to use.

Flow cytometry and cell sorting

Fibroblasts were dissociated using 0.05% trypsin or 1mM EDTA and stained on ice with conjugated antibodies for 25 minutes prior analysis on either an Attune (ThermoFisher) or Quanteon (Agilent) flow cytometer. 1 µg/ml of DAPI was added 10 minutes prior to analysis for dead cell exclusion. See **Supplementary Table 2** for the complete list of antibodies used to profile fibroblasts (data for antibodies in gray are not presented in the manuscript; fibroblasts were uniformly negative for these markers). Unstained cells were used to establish positive and negative gates. FlowJo v.10.6.2 (BD Life Sciences) was used to analyze data. GraphPad Prism v.9.3.1 was used to perform simple linear regression, unpaired t tests with Welch's correction, and 2-way ANOVA with Tukey's multiple comparisons test.

Many experiments (growth curve analysis, RNA-sequencing, adipogenesis, osteogenesis, Luminex, and cocultures) presented in this manuscript necessitated the sorting of cultured fibroblasts into $CD105^+$ and $CD105^-$ subpopulations. Fibroblasts were dissociated using 0.05% trypsin and stained on ice with conjugated antibodies targeting CD105 and in some cases CD26 (**Supplementary Table 2**) for 25 minutes, with rinsing, prior to sorting using an Aria III cell sorter (BD Biosciences). 1 µg/ml of DAPI was added 10 minutes prior to sorting for dead cell exclusion. Unstained cells were used to establish positive and negative gates. Forward scatter (FSC) and side scatter (SSC) were used to identify fibroblasts based on size and granularity. Single cells were selected using FSC-area and FSC-height to exclude doublets. DAPI was used to exclude dead cells. Based on gates set by unstained cells, $CD105^+$ and $CD105^-$ fibroblasts were collected into FACs tubes filled with media.

Growth curve analysis

To initiate the growth curve assay, fibroblasts from the following strains were grown to subconfluency: C073, 169, C023, and C008 (starting passages are listed in **Supplementary Table 1**). Fibroblasts were then sorted into $CD105^+$ and $CD105^-$ subpopulations using an antibody targeting human CD105 (**Supplementary Table 2**) with an ARIA III cell sorter (BD Biosciences).50,000 cells were seeded in triplicate at the start of every passage in a 6-well plate (5,200 cells/cm^2) (CytoOne) and cells were counted at the point the dish became subconfluent. Each replicate was counted using a hemocytometer. Total population doublings (PD) were calculated using the equation $PD = \log2(N^{final}/N^{initial})$. N is the number of cells counted. GraphPad Prism v.9.3.1 was used to perform a 2-way ANOVA on the growth curves from fibroblast subtypes.

Differentiation assays

For adipogenic differentiation sorted $CD105^+$ and $CD105^-$ fibroblasts (**Supplementary Fig. 4**) were seeded at 20,000 cells per well in 12-well plates (5,700 cells/cm^2) (Greiner Cellstar) and changed to adipogenic (100nM dexamethasone (Sigma-Aldrich, D1756), 450uM 1-methyl-3-isobutylxanthine (Sigma-Aldrich, I5879), 1µM Rosiglitazone (Cayman, 71740), and 1µg/ml insulin (Sigma-Aldrich, I5500) in DMEM/F12 (Gibco) + 10%FBS (Gemini Bio-Products)) (31, 32) or control media (DMEM/F12 + 10%FBS) once cells reached subconfluence (typically after 4 days). Adipogenic induction was visualized by Oil Red O (ORO) (Sigma-Aldrich O0625) staining after 2 weeks. Cultures were fixed at room temperature for 15 minutes in 4% paraformaldehyde, cells were rinsed with water, washed with 60% isopropanol (IPA) for 5 minutes, and stained with ORO working solution (0.3 mg/ml Oil Red O dye in 60%IPA) for 20 minutes at room temperature. To quantify ORO staining, cells were rinsed with water, washed with 60% IPA for 5 minutes, and 250µl of 100% IPA was added to each well to solubilize ORO staining. 200µl of the IPA:ORO solution was transferred to a microplate (Corning) and absorbance at 492nm was read on a plate reader (100% IPA was used as a blank). GraphPad Prism v.9.3.1 was used to perform paired T-tests.

For osteogenic differentiation, sorted $CD105^+$ and $CD105^-$ fibroblasts were seeded at 20,000 cells/cm^2, and changed to osteoblastic (5mM beta-glycerophosphate (Sigma-Aldrich G9422), 283µM L-ascorbic acid (Sigma-Aldrich A92902), 10nM dexamethasone (Sigma-Aldrich D1756), and 10µM 1α,25-dihydroxyvitamin D3 (Sigma-Aldrich D1530) in DMEM/F12 (Gibco) + 10%FBS (Gemini Bio-Products))(31) or control media (DMEM/F12 + 10%FBS) after two days in culture. Alizarin Red staining (Abcam) was used to assess formation of mineralized matrix after 4 weeks as described (31). Induction of differentiation in human bone marrow-derived MSCs (ATCC, PCS-500-012) was used as a positive control in both assays.

Luminex assay

100,000 viable sorted $CD105^+$ and $CD105^-$ fibroblasts were seeded into 6-well plates (10,400 cells/cm^2) (CytoOne) in M87A + 5% FBS (Gemini Bio-Products). Media was changed after 2 days. 48 hours after the media change, supernatant was collected and centrifuged at 2,000X g for 10 minutes at 4°C. Cell and debris-free supernatant was stored at -80°C until analysis in duplicate on a custom 23-plex (LUM, ALDH1A1, MMP-3, IL-8, CD26, CXCL6, CCL2, IL-1β, DKK-1, SPARC, CXCL1, M-CSF, TSP-2, POSTN, FN1, BMP-2, IL-6, IL-33, MCAM, IGFBP-2, IGFBP-7, LIF, SCF) Luminex assay (R&D Systems). Concentrations of each analyte were adjusted based on values from M87A + 5%FBS media alone. Values below the detectable range were replaced with zeroes. Values above the detectable range were replaced with N/A values. Concentrations for SPARC, FN1, and ALDH1A1 were outside of reliable detection limits for all strains and were excluded from analysis. To generate the principal component analysis (PCA) plot in R v.4.1.2 (33) (**Supplementary Fig. 4B**), analytes MMP3, CXCL1, and IL8 were also excluded from analysis because of N/A values for some samples. GraphPad Prism v.9.3.1 was used to perform paired T-tests and simple linear regressions.

Bulk RNA-sequencing

Fibroblasts were sorted into $CD105^+$ and $CD105^-$ subpopulations using the markers described above (**Supplementary Fig. 2A**) with an ARIA III cell sorter (BD Biosciences). $CD105^-$ fibroblasts from donor C145 were excluded from downstream analysis as this population represented a relative $CD105^{low}$ group of cells that was not transcriptionally similar to any other $CD105^-$ samples. RNA extraction from the sorted cells was performed using a Quick-RNA Microprep kit with Zymo-Spin IC columns (Zymo Research, catalog no. R1050). Samples were then submitted to COH integrative genomics core for RNA-seq. RNA-seq libraries were prepared using KAPA RNA mRNA HyperPrep Kit (KAPABiosystems, catalog no. KR1352) according to the manufacturer's protocol. Sequencing was performed on an Illumina NovaSeq 6000 with the paired-end read mode of 101 cycles. RNA-seq reads were trimmed to remove sequencing adapters using Trimmomatic (34). The processed reads were mapped back to the human genome (hg19) using TOPHAT2 software (35). HTSeq (36) and RSeQC (37) software packages were applied to generate the count matrices and strand information, respectively, using default parameters. Differential gene expression analysis was performed in R using DESeq2 (38). A vst() transformed DESeq object was used to generate the PCA plot and heatmap (39). Genes labeled on the heatmap are the top 30 genes differentially expressed in $CD105^+$ vs. $CD105^-$ fibroblasts ordered by adjusted p-value with a minimum expression of 100 normalized count values. A lfcShrink() transformed DESeq object was used to generate the Enhancedvolcano plot (40) that was labeled with significantly upregulated genes related to the Gene Ontology (GO) term "negative regulation of immune system" along with *ENG* and *CD248*. topGO (41) was used to perform GO term enrichment analysis on genes significantly upregulated (log2FoldChange > 1 & baseMean > 1 & padj < 0.05) in $CD105^+$ compared to $CD105^-$ fibroblasts. Pathways with Kolmogorov-Smirnov values less than 0.05 were considered significantly enriched (**Supplementary Fig. 2B**). Further pathway analysis was performed with clusterProfiler (42) on differentially expressed genes (log2FoldChange > or < 0 & padj < 0.05) ranked by log2FoldChange. Ingenuity pathway analysis (IPA) (43) of significantly differentially expressed genes (log2FoldChange > 1 or < -1 & baseMean > 1 & padj < 0.05) between $BRCA1^{mut/+}$ $CD105^+$ and younger AR $CD105^+$ fibroblasts was analyzed with the use of QIAGEN IPA.

scRNA-seq analysis

For visualization of gene expression at single-cell resolution and single cell gene set enrichment analysis (scGSEA), three data sets were used: both Kumar et al. 2023 (21) and Reed et al. 2024 (24) were downloaded from CELLXGENE (44) as Seurat objects (45) and GSE161529 (46) was provided as a Seurat object by the group of Dr. Andrea Bild. Downstream analysis was performed on fibroblasts and myeloid cells from the Kumar et al. dataset; stroma and fibroblasts from the Reed et al. dataset, and fibroblasts from the Pal et al. dataset. Data processing and analysis was performed in R. ssCustomize() was used to visualize the expression of single genes and the CD105 signature top 30 differentially expressed genes (> 100 mean normalized count and ordered by adjusted P value) between $CD105^+$ and $CD105^-$ fibroblasts (**Supplementary Table 3**) on UMAPs from each dataset. scGSEA was performed using the escape R package (47) that utilizes UCell (48) to execute and visualize GSEA across individual cells.

Comparisons between cell types and groups were subjected to the Kruskal-Wallis test with post-hoc Wilcoxon to determine p-values. (21). The Kruskal-Wallis test with post-hoc Wilcoxon was used to compare mean signatures between groups and revealed that nearly every comparison was extremely significantly different ($p < 0.0001$), but that was likely a reflection of very small differences amplified by massive sample sizes, thus masking actual biological differences (Fig. 6A**&B, Supplementary Fig. 6B-E, G-I**). For this reason, p-values were not plotted and instead stars represent standardized mean difference calculations. Standardized mean differences were calculated by subtracting the means of two groups and dividing by the pooled standard deviation not accounting for sample size of each group (49). CellChat (v.1.1.3) (50) was applied with default parameters to myeloid cells and fibroblasts from Kumar et al. to infer differential strength and number of interactions between cells differing in menopausal status.

Immunofluorescent staining in cultured fibroblasts

Fibroblasts were seeded onto glass coverslips in 24-well plates (Greiner Cellstar, 662160) at a density of 5,263 cells/cm^2 in M87A + 5%FBS. Fibroblasts were grown until close to confluence, fixed with ice cold methanol:acetone for 15 minutes, blocked with immunofluorescence (IF) blocking buffer (5% donor goat serum (R&D Systems, S13150) and 0.1% Triton X-100 (Sigma-Aldrich T8787) in phosphate-buffered saline (PBS)) for 1 hour at room temperature, incubated with a staining solution with antibodies targeting CD105 and ACTA2 (alpha smooth muscle actin) (**Supplementary Table 4**) overnight at 4°C on a rotating shaker, coverslips were washed with PBS, incubated with a secondary staining solution with Hoechst for 2 hours at room temperature, washed with PBS, and mounted using Fluoromount-G (Electron Microscopy Sciences, 17984). Multiple representative images were acquired for each coverslip using a Nikon Eclipse Ti2. Coverslips only stained with secondary antibodies served as controls and were used to set exposure times for image acquisition. CellProfiler (51) was used to determine the mean intensity of ACTA2 and CD105 for each fibroblast from each strain. Mean intensity values were plotted using geom_pointdensity in R after rescaling values between 0 and 1.

Immunofluorescent staining of tissue sections

Formalin fixed paraffin-embedded (FFPE) tissue sections were deparaffinized and rehydrated by washing slides in xylene 3 times for 3 minutes each, dunking slides 20 times in 3 different 100% ethanol coplin jars, dunking slides 20 times in 2 different 95% ethanol coplin jars, and removing ethanol from each slide by rinsing with diH_2O. Antigen retrieval was performed by incubating the slides with citric acid-based antigen unmasking solution (Vector Laboratories, H-3300) at 98°C for 10 minutes; slides were allowed to cool at room temperature until they reached 35°C. Then, sections were washed with PBS for 5 min. Samples were incubated in IF blocking buffer at room temperature for 1 hour. Primary antibodies targeting CD248, K14 (also listed as KRT14, myoepithelial marker), K19 (also listed as KRT19, luminal marker) (**Supplementary Table 4**) were diluted into IF blocking buffer and incubated with the samples overnight. Samples were washed three times with PBS, stained with appropriate fluorophore-conjugated secondary antibodies (**Supplementary Table 4**) and Hoechst stain 33342 (**Supplementary Table 4**) for 2

hours at room temperature. Slides were washed 3 times with PBS at room temperature and then coverslips were mounted using Fluoromount-G. Multiple representative images of ducts and lobes were acquired using a Nikon Eclipse Ti2 or a Zeiss LSM 700. Fiji (52) was used to select lobular and ductal structures based on keratin staining patterns: lobular structures were characterized by sporadic staining of the luminal marker K19 and sparse staining of myoepithelial marker K14; ductal structures were identified by presence of bilayered epithelium with $K19^+$ luminal cells lining the lumen surrounded by $K14^+$ myoepithelial cells(53). The mean fluorescence intensity of CD248 of a selected region was divided by the average mean fluorescence intensity of the background to determine the relative intensity of CD248 staining for a particular structure. Mann-Whitney test was used to determine whether differences between groups were significant.

Immune cell source

Day of leukapheresis, PBMCs were isolated by density gradient centrifugation over Ficoll-Paque (GE Healthcare) followed by multiple washes with PBS containing 1 mM EDTA (PBS-EDTA, Cellgro). Monocytes were isolated from freshly collected PBMCs using CD14 antibody-conjugated microbeads and magnetic columns (Miltenyi Biotec, 130-050-201) according to the manufacturer's protocol. $CD14^+$ and CD14– fractions were frozen in CryoStor CS5 (StemCell Technologies) in liquid nitrogen until initiation of coculture experiments.

Macrophage differentiation

Primary human pro- and anti-inflammatory macrophages were differentiated and polarized as previously described (54, 55). Briefly, frozen human monocytes ($CD14^+$) were thawed and cultured in cytokine-containing RPMI (Lonza) + 10% FBS (heat-inactivated, gamma-irradiated Hyclone) for 8 days in 6-well plates (104,200 cells/cm^2 seeding density) (CytoOne). To differentiate pro-inflammatory macrophages, cells were cultured with GM-CSF (BioLegend, 572903). The media was changed once after 4 days to media containing GM-CSF, IFN-γ (BioLegend, 570202), LPS (Sigma-Aldrich, L3012) and IL-6 (BioLegend, 570804). To differentiate anti-inflammatory macrophages, cells were cultured with M-CSF (BioLegend, 574804). The media was changed once after 4 days to media containing M-CSF, IL-4 (BioLegend, 574002), IL-13 (BioLegend, 571102) and IL-6. All cytokines and LPS were used at 20 ng/mL. After another 4 days of differentiation, macrophages were dissociated using 1mM PBS-EDTA, and phenotype was assessed by flow cytometry (CD80, CD206, and CD163; **Supplementary Table 2**) and qPCR (**Supplementary Table 5**) to confirm successful polarization. Cells were counted and used for further studies.

Cocultures

After 8 days of macrophage differentiation and polarization, sorted (using the protocol outlined in *Flow cytometry and cell sorting*) $CD105^+$ and $CD105^-$ fibroblasts (see **Supplementary Table 1** for strains and passage numbers) were seeded at a ratio of 1:2.5 (fibroblast:macrophage) onto macrophages that had been washed to remove polarization media (Fig. 4A). Cocultures were maintained for 4 days in RPMI +

10%FBS with a media change at day 2. Macrophages cultured without fibroblasts in base media served as controls. At day 4, fibroblasts and macrophages were dissociated using 1mM EDTA and passed through a 100 µm filter to remove cell aggregates that did not dissociate. Macrophages were separated from fibroblasts using a magnetic bead CD45 positive isolation kit (STEMCELL, 100–0105) according to the manufacturer's protocol.

Triculture experiments were conducted in XVIVO 15 (Lonza) + 10%FBS to maximize T cell viability. Following the two-phase differentiation and polarization protocol, macrophages were profiled by flow cytometry (CD80, CD206, and CD163; **Supplementary Table 2**) and counted. 100,000 macrophages were seeded in each well of a 24-well plate (Greiner Cellstar, 662160). 40,000 sorted (using the protocol outlined in *Flow cytometry and cell sorting*) $CD105^+$ and $CD105^-$fibroblasts (C147, passage 4) were counted and seeded onto adherent macrophages. $CD14^-$ cells were thawed and profiled for $CD3^+$ T cell proportion by flow cytometry (**Supplementary Table 2**). The T cell enriched fraction was labeled with CFSE violet (ThermoFisher, C34571) according to the manufacturer's protocol. T cells were then stimulated with CD3/CD28 Dynabead (ThermoFisher, 11161D) at a ratio of 1 bead to 1 T cell. 100,000 labeled, stimulated T cells were then added to the appropriate wells and coculture was maintained for 3 days prior to analysis of T cell proliferation by flow cytometry. Unstimulated T cells served as a negative control and stimulated T cells alone served as the positive control.

Coculture endpoint analysis

A fraction of macrophages were analyzed by flow cytometry (CD45, CD80, CD163, CD206; **Supplementary Table 2**) and the remaining macrophages were lysed and stored at -80°C until qPCR analysis. Total RNAs were isolated from CD45-enriched macrophages with Quick-RNA Microprep kit (Zymo Research). For qPCR, cDNAs were synthesized with iScirpt reverse transcriptase (Bio-Rad) according to the manufacturer's manual. Quantitative gene-expression analysis was performed by CFX384 real-time PCR (Bio-Rad) with Universal SYBRGreen supermix (Bio-Rad). Data were normalized to *TBP* after calculating relative quantity ($2^{\Delta Cq}$) based on specified control groups. Normalized gene expression was then $\log_2$ transformed. Primers are listed in **Supplementary Table 5**. GraphPad Prism v.9.3.1 was used to perform two-tailed unpaired T-tests.

For macrophage:fibroblast:T cell triculture experiments, T cells in suspension were collected with light pipetting and stained with CD3, CD4, and CD8 targeted antibodies (**Supplementary Table 2**). T cells were gated based on CD3 and either CD4 or CD8 expression. Unstained T cells were used to establish CD3, CD4, and CD8 gates. CFSE-labeled, unstimulated T cells were used to establish the gate for proliferating T cells (**Supplementary Fig. 5G&H**). GraphPad Prism v.9.3.1 was used to perform two-tailed unpaired T-tests.

Results

CD105 expression increases in early passage primary fibroblasts from high-risk women

CD105 expression was used to distinguish between interlobular/ductal ($CD105^{-}$) and lobular ($CD105^{+}$) fibroblasts present in early passage, primary fibroblasts from 30 women (**Supplementary Fig. 1A**). Peri-epithelial primary fibroblast strains from 20 average risk (AR) women ranging in age from 16 to 70 years were established by isolating and sub-culturing the fibroblasts that migrated from epithelial organoids onto the culture plastic surface, when they were purified by differential trypsinization and then sub-cultured. CD105 expression was measured using flow cytometry. A simple linear regression shows a strong positive correlation between age and proportion of fibroblast population that express CD105 (Fig. 1A). Because $CD105^{+}$ fibroblasts were found to be enriched in older women, who are more susceptible to breast cancer, and $CD105^{+}$ fibroblasts have been described as the source of myofibroblast-like cancer associated fibroblasts (myCAFs) that are associated with poor patient outcomes (15), we measured CD105 proportions in another group of women with genetically increased breast cancer susceptibility. Flow cytometry was used to measure CD105 expression in fibroblasts isolated from women with pathogenic *BRCA1* mutations and fibroblasts from these women have significantly (P = 0.026) larger $CD105^{+}$ populations (mean = 83.9%) when compared to their age-matched AR peers (mean = 64.9%) (Fig. 1B). $CD105^{+}$ fibroblasts were reported to have a slower growth rate than their $CD105^{-}$ counterparts (8, 14, 15), and this was found to be true in four strains from different risk groups (Fig. 1C). Taken together, these results indicate that $CD105^{+}$ fibroblasts are enriched in populations at higher risk for breast cancer.

Early passage fibroblasts were uniformly positive for fibroblast markers CD13 (13, 56), CD109, platelet-derived growth factor receptor alpha (PDGFRα), and platelet-derived growth factor receptor beta (PDGFRβ) (57–60) and mesenchymal stem cell (MSC) markers CD73, CD90, CD166, and protein C receptor (PROCR) (61–63)(**Supplementary Fig. 1C**). A marker of CAFs, podoplanin (PDPN), was the only marker found to vary in expression between the three groups analyzed, as $BRCA1^{mut/+}$ fibroblasts had significantly (P = 0.0016) less PDPN than older AR fibroblasts (**Supplementary Fig. 1C**), which agrees with observations made about CAFs derived from women with *BRCA1* mutations (64).

$CD105^{+}$ fibroblasts from women with differences in breast cancer susceptibility differ transcriptionally

To further define differences between $CD105^{+}$ and $CD105^{-}$ fibroblasts and fibroblasts from women with differences in breast cancer susceptibility, RNA-sequencing was performed on sorted fibroblasts from 15 individuals (**Supplementary Fig. 2A**). Sequenced samples predictably separate by CD105 expression in a principal component analysis (Fig. 2A). When samples are clustered by the top 30 differentially expressed genes between $CD105^{+}$ & $CD105^{-}$ three populations emerge: $CD105^{-}$ (with specimen 122 $CD105^{+}$ as the lone outlier in this cluster), $CD105^{middle}$ (C023, 051L, 240, C073, C078, 112, 160, and C051 $CD105^{+}$), and $CD105^{high}$ (C094, C045, 169, 117, C145, and C147 $CD105^{+}$) (Fig. 2B). This data further

supports the idea that there are grades to CD105 expression and it is notable that the $CD105^{high}$ group is composed primarily of older and $BRCA1^{mut/+}$ strains (save for the oldest younger AR strain, 169) (15, 65). A majority of differentially expressed genes between $CD105^+$ & $CD105^-$ fibroblasts are genes that are upregulated in $CD105^+$ fibroblasts. Gene ontology (GO) pathway analysis of the upregulated genes in $CD105^+$ fibroblasts relative to $CD105^-$ fibroblasts found that the most enriched biological process in $CD105^+$ fibroblasts is negative regulation of the immune system (**Supplementary Fig. 2B**). Genes from this pathway that are upregulated in $CD105^+$ fibroblasts are labeled on the volcano plot in Fig. 2C along with *ENG* (*CD105*) and *CD248*, which is a proxy marker for $CD105^+$ fibroblasts Further pathway level analysis of differentially expressed genes shows that $CD105^-$ fibroblasts are enriched for MSigDB hallmark pathways related to proliferation (Fig. 2D **&** Fig. 1C). Genes differentially expressed in $CD105^+$ fibroblasts are enriched in pathways related to myogenesis, adipogenesis, angiogenesis, and TGFβ signaling (Fig. 2D). $CD105^+$ fibroblasts were also enriched for a host of pathways related to inflammation including: inflammatory response, IL6 signaling, IFNγ response, IFNα response, and TNFα signaling which indicates that these fibroblasts are associated with a chronically inflamed microenvironment (Fig. 2D).

Observing transcriptional differences between $CD105^+$ and $CD105^-$ fibroblasts is not novel (8, 65, 66), and we next determined whether $CD105^+$ fibroblast populations differed between individuals with differences in breast cancer susceptibility (Fig. 2E). The greatest number of differentially expressed genes are between $CD105^+$ and $CD105^-$ fibroblasts from individuals in the same risk group; however, a more interesting observation was that $CD105^+$ fibroblasts from women who carry *BRCA1* mutations are transcriptionally distinct from $CD105^+$ fibroblasts from their age-matched AR counterparts (Fig. 2E). Ingenuity pathway analysis (IPA) showed that the top pathways enriched in $CD105^+$ $BRCA1^{mut/+}$ fibroblasts were related to fibrosis, autoimmune diseases, and cytokine storm signaling (Fig. 2F). This result further strengthens the connection between $CD105^+$ fibroblasts and immune modulation and suggests that fibroblasts from women with *BRCA1* mutations may be especially prone to fibrosis and immune cell interactions. $CD105^+$ fibroblasts have a unique transcriptional signature that suggests they have characteristics of myofibroblasts, are capable of transdifferentiating, contribute to inflammation, and may interact with immune populations.

$CD105^+$ fibroblasts are capable of adipogenesis and secrete macrophage polarization factors

Because $CD105^+$ fibroblasts express markers enriched on adipose stem cells *e.g.* CD13, CD73, CD90, PDGFRα, and PDGFRβ (**Supplementary Fig. 1C**) (67, 68), have upregulated expression of genes related to adipogenesis, like *MEDAG* and *EBF1* (69)(Fig. 2B**&D**), and have previously been shown to exhibit adipogenic potential like mesenchymal stem cells (MSCs)(8, 70) we quantified the adipogenic potential of $CD105^+$ fibroblasts from 15 individuals. $CD105^+$ and $CD105^-$ fibroblasts were grown in DMEM/F12 + 10% FBS until they were subconfluent when media was switched to an adipogenic media for 2 weeks.

Following culture in adipogenic media, cells were fixed and neutral lipids were stained with an oil red O (ORO) solution. ORO stained oil fat vacuoles are prominent in $CD105^+$ fibroblasts treated with adipogenic media compared to the background signal in other conditions (Fig. 3A). $CD105^+$ fibroblasts have significantly greater optical density (OD) 492nm values when compared to $CD105^-$ fibroblasts indicating greater adipogenic potential (Fig. 3B). No difference in adipogenic potential between $CD105^+$ fibroblasts from different risk groups was observed and within each group there was large variability in adipogenic potential between $CD105^+$ fibroblasts (**Supplementary Fig. 3A&B**).

Though not statistically significant, the fact that the top three strains with the greatest adipogenic potential are from women older than 55 years of age suggests that fibroblasts may contribute to increased adiposity of the breast with age (71, 72) (**Supplementary Fig. 3B**). Adipogenesis is one assay to identify MSC populations along with osteogenesis and chondrogenesis (61). $CD105^+$ fibroblasts did not exhibit ability to differentiate into osteoblasts when compared to a MSC positive control as measured by Alizarin-red staining (data not shown).

RNA sequencing also suggested that $CD105^+$ fibroblasts exhibit a myofibroblast like state with enrichment of the “Myogenesis” term (Fig. 2D). Despite enrichment of this term, $CD105^+$ fibroblasts regardless of donor did not reliably coexpress alpha smooth muscle actin (ACTA2), a marker of myofibroblasts (73) (Fig. 3C **& Supplementary Fig. 3C**). There was variability between strains in numbers of $ACTA2^+$ fibroblasts present in culture and a trend towards greater expression of ACTA2 in cells that had lower levels of CD105 expression (**Supplementary Fig. 3C**).

The discordance between mRNA and protein abundance makes it challenging to define essential components of a niche using RNA-sequencing alone (74). To combat this issue, a majority of the analytes selected to be measured using a custom Luminex panel were the protein products of significantly differentially expressed genes between $CD105^+$ and $CD105^-$ fibroblasts (75). The remaining analytes measured were selected because they were either associated with immune modulation or had been previously reported to be associated with $BRCA1^{mut/+}$ fibroblasts (e.g. MMP3) (76). Six of the 19 analytes measured within detectable ranges differed in abundance between $CD105^+$ and $CD105^-$ fibroblasts (Fig. 3D). Strains clustered by CD105 expression when analyzed by PCA as was observed using RNA (**Supplementary Fig. 4A&B;** Fig. 2A). All 6 differentially secreted proteins by $CD105^+$ fibroblasts are involved in either the establishment of an immunosuppressive microenvironment or the direct polarization of macrophages towards an anti-inflammatory phenotype (Fig. 3D) (77–85). Closer consideration of the effects of proteins produced by $CD105^+$ fibroblasts suggest a tension in maintaining the $CD105^+$ state. While POSTN can increase the proliferation and ACTA2 expression of myofibroblasts (86), both DKK1 and CCL2 inhibit myofibroblast differentiation and may explain why the sequencing data does not match ACTA2 expression in cultured cells (Fig. 2D, Fig. 3C) (87, 88). A similar story emerges when contrasting TSP2, a potent inhibitor of angiogenesis (81), with IGFBP-2, a protein that supports angiogenesis and the migration of endothelial cells (83). The 6 proteins with increased abundance in the

supernatant derived from CD105$^+$ fibroblasts compared to CD105$^-$ fibroblasts had significant correlation between RNA and protein level data (Fig. 3E). For the proteins that did not differ in abundance between fibroblast subtypes, only 3 of 13 had a significant correlation between RNA and protein expression (**Supplementary Fig. 4C&D**). The Luminex data suggest CD105$^+$ fibroblasts have immunosuppressive characteristics, may influence myofibroblast differentiation, and may be involved in remodeling vasculature.

Fibroblast subtypes influence immune cell polarization and function

We next assessed whether CD105$^+$ fibroblasts established an immunosuppressive microenvironment by influencing the polarization of macrophages. Primary cocultures were established leveraging a previously published protocol for differentiating pro- and anti-inflammatory macrophages from primary monocytes (Fig. 4A) (55). After differentiation/polarization (Fig. 4A), pro-inflammatory macrophages express CD80 and anti-inflammatory macrophages uniformly express CD206 and CD163 (**Supplementary Fig. 5A**). After 4 days of direct coculture between differentially polarized macrophages and sorted fibroblasts (**Supplementary Fig. 5B**), CD80 expression is completely lost in all conditions (data not shown). CD206 is significantly induced and suppressed in pro- and anti-inflammatory macrophages, respectively, when cocultured with fibroblasts (Fig. 4B, **left**). There is a trend towards increased CD163 expression in pro-inflammatory macrophages with fibroblast coculture and a significant increase in CD163 expression in anti-inflammatory macrophages cocultured with CD105$^+$ fibroblasts compared to anti-inflammatory macrophages after 4 days without polarization media (Fig. 4B, **right**).

After 4 days of coculture with fibroblast subtypes, macrophages were isolated using magnetic bead enrichment for CD45. This method yields a pure macrophage population with good viability (**Supplementary Fig. 5C&D**). Expression of pro-inflammatory genes were then assessed by qPCR (Fig. 4C**)**. *TNFα* expression decreases in pro-inflammatory macrophages after 4 days of culture but is significantly further decreased by coculture with CD105$^+$ fibroblasts. *IL1β* expression also decreases in culture for pro-inflammatory macrophages; however, anti-inflammatory macrophages cocultured with fibroblasts significantly increase the expression of this pro-inflammatory gene. *CXCL1* expression is maintained at baseline (D0) levels by fibroblast coculture in pro-inflammatory macrophages and induced in anti-inflammatory macrophages cocultured with fibroblasts. *IL6* expression also increases relative to monoculture in both macrophage subtypes cocultured with fibroblasts. Immediate and transient expression of these pro-inflammatory cytokines is essential for response to environmental stressors, and chronic expression can contribute to immune exhaustion and disease states (89, 90). Expression of anti-inflammatory genes was also measured (Fig. 4D). *IL10* expression is increased in pro-inflammatory macrophages after 4 days regardless of culture condition, but expression is significantly increased in anti-inflammatory macrophages cocultured with fibroblasts. *CD206* increases in expression in pro-inflammatory macrophages cocultured with fibroblasts to the same level as freshly polarized anti-inflammatory macrophages which agrees with protein level expression (Fig. 4B, **left)**. CD105$^-$ fibroblasts

significantly increase the expression of *CD206* in anti-inflammatory macrophages which according to new research, may actually improve adaptive immune surveillance of tissue (91). *CD163* expression increases in expression in pro-inflammatory macrophages cocultured with fibroblasts to a level that is similar to D4 anti-inflammatory macrophages in monoculture. Surprisingly, when considering protein level expression (Fig. 4B, **right)**, *CD163* expression decreases in anti-inflammatory macrophages in coculture with fibroblasts. *FN1* expression is lost in culture in anti-inflammatory macrophages, but fibroblast coculture can induce expression in pro-inflammatory macrophages to levels akin to freshly polarized anti-inflammatory macrophages and expression is maintained in anti-inflammatory macrophages cocultured with fibroblasts. Fibroblast coculture increased expression of genes relevant to tumor-associated macrophages (Fig. 4E**)** (92–94). *CXCL12* expression was significantly increased in pro-inflammatory macrophages cocultured with $CD105^-$ fibroblasts and fibroblast culture regardless of CD105 expression increased *CXCL12* expression in anti-inflammatory macrophages. The expression of the cognate receptor for *CXCL12, CXCR4*, only increased in anti-inflammatory macrophages cocultured with fibroblasts. *IL33* expression was induced in anti-inflammatory macrophages cocultured specifically with $CD105^+$ fibroblasts. This cytokine has been associated with anti-inflammatory macrophages contributing to Th2 immune responses as well as the expansion and immunosuppressive function of myeloid-derived suppressor cells (MDSCs) in the tumor microenvironment (95, 96). We find that these peri-epithelial fibroblasts maintain and enhance macrophage polarization.

A more effective readout of a macrophage's polarization state is its functional ability to inhibit T cell proliferation. Primary tricultures were established between CD3/CD8 stimulated T cells, polarized macrophages, and sorted fibroblasts (Fig. 5A). Triculture did not influence the composition of $CD4^+$ and $CD8^+$ T cells in culture (Fig. 5B). Proliferative clusters were observed when T cells were stimulated with CD3/CD28 beads and when stimulated T cells were cultured with pro-inflammatory macrophages (**Supplementary Fig. 5E**). T cells labeled with a CellTrace dye were removed from culture after 3 days and proliferation was measured by quantifying dilution of dye. Most cells in suspension were $CD3^+$ (**Supplementary Fig. 5F**). Around 40% of both $CD4^+$ and $CD8^+$ T cells are proliferating after 3 days in culture (Fig. 5C**&D**). Both pro- and anti-inflammatory macrophages suppress the proliferation of stimulated T cells in culture, but the suppressive effect anti-inflammatory macrophages have on proliferation of T cell subtypes is greater than that of pro-inflammatory macrophages (Fig. 5C**&D**). There is a non-significant trend of decreased proliferation in T cells cultured with pro-inflammatory macrophages and $CD105^+$ fibroblasts compared to T cells in combination with $CD105^-$ fibroblasts (Fig. 5C**&D**). Anti-inflammatory macrophages dramatically suppress the proliferation of T cells, which is apparent when viewing representative histograms of CellTrace dilution (**Supplementary Fig. 5G&H**). An enhancement of this immunosuppressive phenotype would be difficult to detect, but $CD105^-$ fibroblasts reduce the ability of anti-inflammatory macrophages to suppress $CD4^+$ T cell proliferation relative to anti-inflammatory macrophages alone (Fig. 5C). $CD105^+$ fibroblasts maintain the ability of anti-inflammatory macrophages to suppress $CD4^+$ T cell proliferation (Fig. 5C). $CD105^+$ fibroblasts maintain the

immunosuppressive effects of anti-inflammatory macrophages and coax pro-inflammatory macrophages towards a more anti-inflammatory phenotype.

The CD105$^+$ signature identifies macrophage-interacting fibroblasts that increase in postmenopausal women.

To assess the *in vivo* relevance of the conclusions drawn from analyzing cultured CD105$^+$ fibroblasts, we performed single-cell gene set enrichment analysis (scGSEA) using UCell (48) on publicly available scRNA-seq datasets from human breast tissue (21, 24, 46). The top 30 differentially expressed genes between CD105$^+$ and CD105$^-$ fibroblasts (Fig. 2B) comprise the CD105$^+$ fibroblast signature (Fig. 6A**&B, Supplementary Fig. 6A-I**) that is more effective at identifying specific cell types and subtypes than single genes (*ENG & CD248*) (**Supplementary Fig. 6A&F**). Enrichment of the CD105 signature is greatest in the fibro-prematrix subtype of fibroblasts from Kumar et al., which through spatial transcriptomics were found to be enriched around TDLUs (Fig. 6A). In this same dataset, the CD105 signature was also enriched in fibroblasts from postmenopausal women and women with dense breasts (Fig. 6B, **Supplementary Fig. 6C**). Also in this dataset, the signature was decreased in fibroblasts from underweight women and women of Asian descent (**Supplementary Fig. 6B&D**). A technical observation from the preparation of single cell suspensions for the Kumar et al. dataset is that the CD105 signature is most enriched in fibroblasts from tissues dissociated for the shortest period, and enrichment decreases with increasing dissociation time (**Supplementary Fig. 6E**). Leveraging another dataset that has tissue from both AR and *BRCA1* mutation carriers, the CD105 signature was enriched in fibroblast subtypes FB1 and FB2 which were both found to increase with age and parity (**Supplementary Fig. 6F**) (24). Considering CD105 expression in flow data (Fig. 1A), it was surprising that fibroblasts from *BRCA1* mutation carriers were not found to be enriched for the CD105 signature and in another dataset (46), *BRCA1$^{mut/+}$* fibroblasts had decreased enrichment of the signature (**Supplementary Fig. 6H&I**). Cell:cell interactions between fibroblast and innate immune cell subtypes were investigated using CellChat (50). The number and strength of interactions between M2 (anti-inflammatory) macrophages and fibro-prematrix fibroblasts increase in postmenopausal women with a concurrent decrease in the interactions between M1 (pro-inflammatory) macrophages and fibro-prematix fibroblasts in these women (Fig. 6C). All prior scRNA-seq analysis was performed on preneoplastic fibroblasts. Leveraging a publicly available dataset comprised of CAFs from different breast cancer subtypes (46), the CD105 signature was found to be most enriched in CAFs associated with triple-negative breast cancer (TNBC) (**Supplementary Fig. 6I**). TNBCs are often characterized by abundant infiltration of tumor associated macrophages that exhibit immunosuppressive effects (97, 98). Further research is needed to determine if CD105$^+$ CAFs in TNBC contribute to this aspect of the tumor microenvironment. scRNA-seq analysis revealed the CD105 signature established from cultured fibroblasts can identify a fibroblast subpopulation enriched around TDLUs, that increases in postmenopausal women and has increased communication with anti-inflammatory macrophages.

Continuing our efforts to relate observations made in primary fibroblasts back to the tissue, we sought to measure the expression of CD105 in tissue sections. Unfortunately, because the CD105 epitope is sensitive to formalin fixation, we were unable to measure expression in FFPE sections that come from some of the same donors as the fibroblast strains analyzed. To remedy this, CD248, which is highly upregulated in $CD105^+$ fibroblasts (Fig. 2C), and has previously been described as a proxy marker for CD105 (14) with comparable enrichment in TDLUs as CD105 (8), was used to identify intralobular fibroblasts *in situ*. Lobules and ducts were identified in tissue sections by morphology and keratin expression in epithelial cells (**Supplementary Fig. 6J**) and relative intensity of CD248 was then measured in 12 specimens (**Supplementary Fig. 6K**). Stromal cells surrounding ducts with clear delineation between myoepithelial ($K14^+$) and luminal ($K19^+$) cells had lower expression of CD248 compared to lobules that are characterized by sporadic K19 and K14 expression (Fig. 6D **left panel**). CD248 expression was significantly higher in lobules compared to ducts, but did not differ in expression in either structure between AR and *BRCA1* mutation carriers (Fig. 6D **right panel**).

Discussion

We previously introduced the concept of accelerated aging in the epithelial compartment of women who possessed clinically relevant *BRCA1* mutations (99, 100). It was not known whether this phenomenon extended beyond the parenchyma. In this manuscript we demonstrate that in younger women, the distribution of $CD105^+$ and $CD105^-$ fibroblasts is about an equal ratio, but with age, this distribution skews towards $CD105^+$ fibroblasts. We observed a similar trend in fibroblasts from younger women with *BRCA1* mutations that is consistent with the idea of accelerated aging of the stroma. $CD105^+$ fibroblasts were found to be a stable population in culture and are enriched for genes related to negative regulation of the immune system, angiogenesis, myogenesis, and adipogenesis. There are transcriptional differences between $CD105^+$ fibroblasts from average risk and $BRCA1^{mut/+}$ donors – $BRCA1^{mut/+}$ $CD105^+$ fibroblasts are enriched for genes related to fibrosis and chronic inflammatory disorders. An essential aspect of the results we report is the experimental validation of the significance of pathways related to adipogenesis and negative regulation of the immune system.

$CD105^+$ fibroblast-specific effects on macrophages include: increasing expression of CD163 in anti-inflammatory macrophages, suppressing *TNFα* expression in pro-inflammatory macrophages, increasing *IL33* expression in anti-inflammatory macrophages, and maintaining anti-inflammatory macrophage-mediated suppression of CD4 T cell proliferation. The association between $CD105^+$ fibroblasts and anti-inflammatory macrophages extended beyond the dish as fibroblast subpopulations from postmenopausal women found to be enriched for the $CD105^+$ signature had increased interactions with anti-inflammatory (M2) macrophages and fewer interactions with pro-inflammatory (M1) macrophages when compared to their premenopausal counterparts. The aged stroma may increase susceptibility to breast cancer as it becomes more adipogenic and immunosuppressive (Fig. 6E).

Reed et al. reported changes to the proportions of populations that were conserved between women with WT and mutant *BRCA1* genotypes. A unique feature of the *BRCA1*$^{mut/+}$ microenvironment was the increased infiltration of CD8$^+$ T cells and the increased expression of *PDL1* on luminal cells and macrophages that would combine to describe an exhausted immune microenvironment ripe for immune escape (24). Increased median cell density of CD8$^+$ and CD4$^+$ T cells in the normal/benign breast lobules of *BRCA* (*BRCA1 or BRCA2*) mutation carriers compared to average risk women was reported (101). In that study population comprised primarily of women < 55 years of age, lobules of *BRCA* mutation carriers not only had increased numbers of T cells compared to average risk counterparts, but also CD68$^+$ macrophages and CD11c$^+$ dendritic cells. When aging is taken into consideration, mean density of CD3$^+$ T cells decline with age only in high-risk women (22). Increased immune infiltration in women carrying *BRCA1* mutations was attributed to increased mutational burden leading to the formation of neoantigens (102). In the present study, cultured CD105$^+$ fibroblasts were shown to influence macrophage polarization and maintain macrophage's ability to suppress T cell proliferation. Future work should directly address how CD105$^+$ fibroblasts may directly recruit T cells through CCL2 (Fig. 2C) or in combination with macrophages due to the expression of *CXCL12* (Fig. 4E).

BRCA1-associated cancers, especially TNBC, are characterized by increased infiltration of tumor-promoting immunosuppressive macrophages, CD4$^+$ T_{regs}, and exhausted T cells (20, 103, 104). How CAFs contribute to this immune microenvironment is an active field of study. CD105$^+$ CAFs in the murine pancreas were found to be tumor permissive whereas CD105$^-$ CAFs were able to support anti-tumor immunity *in vivo* mediated through T and B cells (66). Beyond immunosuppression, CD105$^+$ CAFs have been shown to differentiate cancer cells and increase their metastatic potential in models of cancer in the prostate and colon (65, 105). In the breast, CD105$^+$ CAFs are associated with metastatic recurrence and increased tumor size (9) as well as being prognostic markers for bone metastasis in early breast cancer patients (10). Even though the CD105$^+$ fibroblast signature is enriched in TNBC CAFs and not in CAFs from other subtypes (**Supplementary Fig. 6I**), CD105$^+$ CAFs are still relevant to the other breast cancer subtypes that are more associated with aging. Morsing et al. originally described the division of inter- from intralobular fibroblasts using both CD105 and CD26 to mark subpopulations (8). As reported in this manuscript, they also described CD105$^+$/CD26$^-$ fibroblasts to be slow growing, transcriptionally similar to tumor stroma (myofibroblast-like), have adipogenic and osteogenic differentiation capacity, and support luminal outgrowth which is dependent on TGFβ activity (8, 14). Building on this foundation, they found that CD105$^-$/CD26$^+$ fibroblasts support myoepithelial differentiation and bipotent progenitor cell activity (14). Most recently, CD105 expression was found to mark myCAFs and absence of expression in iCAFs from ER$^+$ breast cancers (15). Collectively, these findings highlight the complexity of fibroblast heterogeneity in shaping the tumor microenvironment and emphasize the need to target specific fibroblast populations, especially in aging-related breast cancers.

Defining fibroblast subtypes is an important pursuit because it allows for greater understanding about normal niches, precancerous niches, and the cell of origin for CAFs. A population of PROCR$^+$/

ZEB1$^+$/PDGFRα$^+$ (PZP) fibroblasts are enriched in African American breast tissues (106). Like the CD105$^+$/CD26$^-$ fibroblasts, these PZP fibroblasts were capable of adipogenic and osteogenic differentiation and when cocultured with epithelial cells allowed for luminal progenitor basalization (106). This fibroblast subpopulation was found to secrete factors also related to polarization of anti-inflammatory macrophages like CXCL12, HGF, CSF1, and POSTN (107, 108). Where these researchers found heterogeneity in PROCR and PDGFRα expression, the fibroblasts analyzed in this manuscript had ubiquitous expression of both markers. This is the great challenge of defining subsets of fibroblasts in culture and efforts should be made to define populations first in tissue using spatial transcriptomics and multi-omics approaches. A more holistic understanding of fibroblasts in native states must begin in tissue and can be supplemented by investigation in culture.

A strength of this manuscript is the number of strains used in each experiment. Only through profiling so many strains from donors differing in age and *BRCA1* status can the variability between individuals be appreciated and trends emerge. Transcriptional profiling of cells can provide valuable insights into pathways that are differentially activated in one cell type vs. another; however, sequencing results can often produce more candidate genes than are experimentally tractable. Top gene candidates found to be differentially expressed between CD105$^+$ and CD105$^-$ fibroblasts were explored at the protein level either through ACTA2 staining or through Luminex assay. Six of the 23 analytes measured were found to be significantly differentially secreted by CD105$^+$ fibroblasts when compared to matched CD105$^-$ fibroblasts. These six analytes all were associated with the establishment of an immunosuppressive niche and this manuscript explored the interaction between fibroblast subtypes in the breast and immune cells which up to this point had yet to be attempted in culture. Cocultures between CAFs and immune cells are well-trodden, but the novelty of this manuscript is that it explores the interactions between normal fibroblasts and immune cells from healthy donors. Rather than relying on non-physiological concentrations of pleiotropic cytokines, direct cocultures likely provide a more realistic insight into how stromal cells may influence immune subpopulations. The confusion in interpreting the results of the fibroblast:macrophage coculture experiments highlights the importance of moving beyond a false M1/M2 dichotomy (109). The CD105 phenotype established and explored here in culture identifies a subpopulation of fibroblasts *in vivo* that increase in older women and are enriched around TDLUs.

Should there be further support in the future for the expansion of CD105$^+$ fibroblasts as contributing factors to breast cancer susceptibility, this population or the proteins secreted by these fibroblasts could be directly targeted. Carotuximab, a humanized monoclonal antibody developed to inhibit angiogenesis by targeting CD105, has been used in clinical trials to target CD105$^+$ CAFs in metastatic, castration resistant prostate cancer (110). Far-fetched prevention studies can be imagined that would use this therapeutic to reshape the composition of fibroblasts in the disease-free breast of women at high risk of developing breast cancer. POSTN production was enriched in CD105$^+$ fibroblasts and may be able to be targeted by administration of Warfarin, which was been shown to reduce the production of Gla domain containing proteins (111). Another, preventative therapeutic option is the targeted, short-term

administration of ibuprofen or similar NSAIDS to reduce the ability of fibroblasts to establish an immunosuppressive niche (112). Preventing deleterious fibroblast subpopulations from expanding could be more effective than targeting CAFs which likely arise from the same tissue resident fibroblast populations (11, 15).

While sample number is a strength of this paper, it is also paradoxically a weakness. Differences between $CD105^+$ and $CD105^-$ fibroblasts were often subtle. It was only with increased sample number that differences between younger and older luminal cells could be appreciated (113, 114). As the experiments reported here were unable to detect significant differences between younger (n = 6) and older (n = 5) fibroblasts, increasing the sample number may be the only way to reveal differences between younger and aged stromal niches. While fibroblasts had an impact on macrophage polarization, very few differences were observed between how different fibroblast subtypes polarize macrophages. A major challenge during coculture experiments was optimizing media conditions for all cell types. Media conditions that supported macrophage and T cell growth were suboptimal, even inhibitory, for fibroblast proliferation and morphology and vice versa. These challenges with the media may have blunted the true impact of different fibroblast subtypes. Finally, CD105 expression was difficult to detect both in scRNA-seq data as well as in FFPE tissue sections. Low expression of CD105 in fibroblasts in scRNA-seq was remedied by implementing a CD105 signature. CD248 served as a proxy marker for CD105 in tissue; however, $CD248^+$ fibroblasts may not directly overlap with $CD105^+$ fibroblasts which would explain the discrepancy between increased $CD105^+$ fibroblast proportion in cultured fibroblasts from women with *BRCA1* mutations that was not mirrored by CD248 expression in tissue sections.

Future experiments are required to identify the most important factors secreted by fibroblast subtypes related to the establishment of an immunosuppressive niche. These factors may be proteins as analyzed in this paper using an ELISA based assay or these factors may be exosomes or metabolic byproducts. Robust enough phenotypes were not observed to merit downstream mechanistic studies. Similarly challenging experiments should be conducted to understand the impact of fibroblasts on endothelial cells and angiogenesis. Finally, future approaches to define fibroblast heterogeneity should take into consideration menstrual cycle phase (2, 115, 116) and move beyond the use of one or two cell surface markers to define complex and dynamic fibroblast populations.

Conclusions

$CD105^+$ fibroblasts increase in proportion with age and in women with *BRCA1* mutations. These fibroblasts are enriched for genes related to myCAFs and negative regulation of the immune system and there are transcriptional differences between $BRCA1^{mut/+}$ and $BRCA1^{WT}$ $CD105^+$ fibroblasts. $CD105^+$ fibroblasts secrete proteins related to the establishment of an anti-inflammatory and angiogenic niche. Macrophages cocultured with fibroblasts better maintain their polarization states with $CD105^+$ fibroblasts promoting the expression of CD163 and *IL33* in anti-inflammatory macrophages. The CD105 transcriptional pattern defined in culture is relevant to *in vivo* conditions and identifies a subset of

fibroblasts enriched in postmenopausal women that have increased interactions with anti-inflammatory macrophages when compared to fibroblasts derived from premenopausal women. Understanding the function of $CD105^+$ fibroblasts in the preneoplastic niche is essential as $CD105^+$ CAFs are associated with such poor patient outcomes. Coculture models like the ones presented in this manuscript may allow for cell:cell interactions involved in establishing TDLUs that are at high risk of cancer initiation to be studied and manipulated in the dish.

Abbreviations

Terminal ductal lobular units (TDLUs)

Extracellular matrix (ECM)

Regulatory T cells (Tregs)

Human mammary epithelial cell (HMEC)

Population doublings (PD)

Oil Red O (ORO)

Isopropanol (IPA)

Gene ontology (GO)

Ingenuity pathway analysis (IPA)

Single cell gene set enrichment analysis (scGSEA)

Phosphate-buffered saline (PBS)

Average risk (AR)

Myofibroblast-like cancer associated fibroblasts (myCAFs)

Mesenchymal stem cell (MSC)

Principal component anlysis (PCA)

Optical density (OD)

Myeloid-derived supressor cells (MDSCs)

Triple-negative breast cancer (TNBC)

PROCR+/ZEB1+/PDGFRα+ (PZP)

Declarations

Ethics approval and consent to participate

The present study was approved by the Human Subjects Committee and the Institutional Review Board (IRB) (17185) at City of Hope. Women were consented in person and sequentially; all women signed a City of Hope IRB-approved consent before trial entry. Breast organoids from reduction mammoplasties were prepared at the Lawrence Berkeley National Laboratory (Berkeley, CA) with approved IRB for sample distribution and collection from specific locations. Leukapheresis products (whole blood discard kits) were obtained from consented healthy donors under protocols approved by the City of Hope Internal Review Board.

Consent for publication

Not applicable.

Availability of data and materials

The authors assert that data supporting the findings of this study not present within the paper or its supplementary information files will be made available upon request. Fibroblast strains are made available either by contacting the corresponding author at City of Hope, or by contacting Dr. Martha Stampfer at http://hmec.lbl.gov.

Competing interests

The authors declare that they have no competing interests.

Funding

This work was supported by awards from the NIH: EB024989,U01CA244109, R33AG059206, R01EB024989, R01CA237602; Department of Defense/Army Breast Cancer Era of Hope Scholar Award (BC141351); Circle 1500; and City of Hope Center for Cancer and Aging to M.A.L.; and E.G.C. is a CIRM Scholar supported by the California Institute for Regenerative Medicine (EDU4-12772). Research reported in this publication included work performed in the Analytical Cytometry, Analytical Pharmacology, and Integrative Genomics Cores supported by the National Cancer Institute of the National Institutes of Health under grant number P30CA033572. The content is solely the responsibility of the authors and does not necessarily represent the official views of the National Institutes of Health.

Authors' contributions

E.G.C. and M.A.L. conceived the study; E.G.C., Y.Y., S.P., and M.A.L. designed the experiments; E.G.C., J.C.L., Y.Y., and J.G. performed the experiments; E.G.C. and Y.Y. analyzed and interpreted the data; E.G.C. wrote the manuscript. All authors read and approved the final manuscript.

Acknowledgements

The authors would like to thank patient advocates Susan Samson and Sany Preto for their consistent input.

References

1. Howard BA, Gusterson BA. Human breast development. J Mammary Gland Biol Neoplasia. 2000;5(2):119-37.
2. Ferguson JE, Schor AM, Howell A, Ferguson MW. Changes in the extracellular matrix of the normal human breast during the menstrual cycle. Cell Tissue Res. 1992;268(1):167-77.
3. Neville M. Anatomy and Physiology of Lactation. Pediatric clinics of North America. 2001;48:13-34.
4. Jindal S, Narasimhan J, Borges VF, Schedin P. Characterization of weaning-induced breast involution in women: implications for young women's breast cancer. npj Breast Cancer. 2020;6(1):55.
5. Tabár L, Dean PB, Tucker FL, Yen AM-F, Fann JC-Y, Lin AT-Y, et al. Breast cancers originating from the terminal ductal lobular units: In situ and invasive acinar adenocarcinoma of the breast, AAB. European Journal of Radiology. 2022;152:110323.
6. Wellings S, Jensen H, Marcum R. An atlas of subgross pathology of the human breast with special reference to possible precancerous lesions. Journal of the National Cancer Institute. 1975;55(2):231-73.
7. Atherton AJ, Monaghan P, Warburton MJ, Robertson D, Kenny AJ, Gusterson BA. Dipeptidyl peptidase IV expression identifies a functional sub-population of breast fibroblasts. International journal of cancer. 1992;50(1):15-9.
8. Morsing M, Klitgaard MC, Jafari A, Villadsen R, Kassem M, Petersen OW, et al. Evidence of two distinct functionally specialized fibroblast lineages in breast stroma. Breast Cancer Research. 2016;18(1):108.
9. Martinez LM, Labovsky V, de Luján Calcagno M, Davies KM, Rivello HG, Bianchi MS, et al. CD105 Expression on CD34-Negative Spindle-Shaped Stromal Cells of Primary Tumor Is an Unfavorable Prognostic Marker in Early Breast Cancer Patients. PloS one. 2015;10(3):e0121421.
10. Giorello MB, Martinez LM, Borzone FR, Padin MDR, Mora MF, Sevic I, et al. CD105 expression in cancer-associated fibroblasts: a biomarker for bone metastasis in early invasive ductal breast cancer patients. Frontiers in cell and developmental biology. 2023;11:1250869.
11. Houthuijzen JM, De Bruijn R, Van Der Burg E, Drenth AP, Wientjens E, Filipovic T, et al. CD26-negative and CD26-positive tissue-resident fibroblasts contribute to functionally distinct CAF subpopulations in breast cancer. Nature Communications. 2023;14(1):183.
12. Yoshitake R, Chang G, Saeki K, Ha D, Wu X, Wang J, et al. Single-Cell Transcriptomics Identifies Heterogeneity of Mouse Mammary Gland Fibroblasts With Distinct Functions, Estrogen Responses, Differentiation Processes, and Crosstalks With Epithelium. Frontiers in cell and developmental biology. 2022;10:850568.

13. Atherton AJ, O'Hare MJ, Buluwela L, Titley J, Monaghan P, Paterson HF, et al. Ectoenzyme regulation by phenotypically distinct fibroblast sub-populations isolated from the human mammary gland. Journal of Cell Science. 1994;107(10):2931-9.
14. Morsing M, Kim J, Villadsen R, Goldhammer N, Jafari A, Kassem M, et al. Fibroblasts direct differentiation of human breast epithelial progenitors. Breast Cancer Research. 2020;22(1):102.
15. Bagger MM, Sjölund J, Kim J, Kohler KT, Villadsen R, Jafari A, et al. Evidence of steady-state fibroblast subtypes in the normal human breast as cells-of-origin for perturbed-state fibroblasts in breast cancer. Breast Cancer Research. 2024;26(1):11.
16. Dawson CA, Pal B, Vaillant F, Gandolfo LC, Liu Z, Bleriot C, et al. Tissue-resident ductal macrophages survey the mammary epithelium and facilitate tissue remodelling. Nature cell biology. 2020;22(5):546-58.
17. Cansever D, Petrova E, Krishnarajah S, Mussak C, Welsh CA, Mildenberger W, et al. Lactation-associated macrophages exist in murine mammary tissue and human milk. Nature Immunology. 2023;24(7):1098-109.
18. Zhou Y, Ye Z, Wei W, Zhang M, Huang F, Li J, et al. Macrophages maintain mammary stem cell activity and mammary homeostasis via TNF-α-PI3K-Cdk1/Cyclin B1 axis. npj Regenerative Medicine. 2023;8(1):23.
19. Mantovani A, Sica A, Sozzani S, Allavena P, Vecchi A, Locati M. The chemokine system in diverse forms of macrophage activation and polarization. Trends in immunology. 2004;25(12):677-86.
20. Mehta AK, Cheney EM, Hartl CA, Pantelidou C, Oliwa M, Castrillon JA, et al. Targeting immunosuppressive macrophages overcomes PARP inhibitor resistance in BRCA1-associated triple-negative breast cancer. Nature Cancer. 2021;2(1):66-82.
21. Kumar T, Nee K, Wei R, He S, Nguyen QH, Bai S, et al. A spatially resolved single-cell genomic atlas of the adult human breast. Nature. 2023;620(7972):181-91.
22. Zirbes A, Joseph J, Lopez JC, Sayaman RW, Basam M, Seewaldt VL, et al. Changes in Immune Cell Types with Age in Breast are Consistent with a Decline in Immune Surveillance and Increased Immunosuppression. Journal of Mammary Gland Biology and Neoplasia. 2021;26(3):247-61.
23. Nee K, Ma D, Nguyen QH, Pein M, Pervolarakis N, Insua-Rodríguez J, et al. Preneoplastic stromal cells promote BRCA1-mediated breast tumorigenesis. Nature genetics. 2023;55(4):595-606.
24. Reed AD, Pensa S, Steif A, Stenning J, Kunz DJ, Porter LJ, et al. A single-cell atlas enables mapping of homeostatic cellular shifts in the adult human breast. Nature genetics. 2024;56(4):652-62.
25. Zhou J, Wang XH, Zhao YX, Chen C, Xu XY, Sun Q, et al. Cancer-Associated Fibroblasts Correlate with Tumor-Associated Macrophages Infiltration and Lymphatic Metastasis in Triple Negative Breast Cancer Patients. J Cancer. 2018;9(24):4635-41.
26. Ben-Chetrit N, Niu X, Sotelo J, Swett AD, Rajasekhar VK, Jiao MS, et al. Breast Cancer Macrophage Heterogeneity and Self-renewal are Determined by Spatial Localization. bioRxiv. 2023.
27. Comito G, Giannoni E, Segura C, Barcellos-de-Souza P, Raspollini M, Baroni G, et al. Cancer-associated fibroblasts and M2-polarized macrophages synergize during prostate carcinoma

progression. Oncogene. 2014;33(19):2423-31.
28. Gok Yavuz B, Gunaydin G, Gedik ME, Kosemehmetoglu K, Karakoc D, Ozgur F, et al. Cancer associated fibroblasts sculpt tumour microenvironment by recruiting monocytes and inducing immunosuppressive PD-1+ TAMs. Scientific reports. 2019;9(1):3172.
29. LaBarge MA, Garbe JC, Stampfer MR. Processing of Human Reduction Mammoplasty and Mastectomy Tissues for Cell Culture. JoVE. 2013(71):e50011.
30. Lee JK, Bloom J, Zubeldia-Plazaola A, Garbe JC, Stampfer MR, LaBarge MA. Different culture media modulate growth, heterogeneity, and senescence in human mammary epithelial cell cultures. PloS one. 2018;13(10):e0204645.
31. Jafari A, Siersbaek MS, Chen L, Qanie D, Zaher W, Abdallah BM, et al. Pharmacological Inhibition of Protein Kinase G1 Enhances Bone Formation by Human Skeletal Stem Cells Through Activation of RhoA-Akt Signaling. Stem cells (Dayton, Ohio). 2015;33(7):2219-31.
32. Fink T, Zachar V. Adipogenic Differentiation of Human Mesenchymal Stem Cells. In: Vemuri M, Chase LG, Rao MS, editors. Mesenchymal Stem Cell Assays and Applications. Totowa, NJ: Humana Press; 2011. p. 243-51.
33. Team RC. R: A language and environment for statistical computing. Foundation for Statistical Computing, Vienna, Austria. 2013.
34. Bolger AM, Lohse M, Usadel B. Trimmomatic: a flexible trimmer for Illumina sequence data. Bioinformatics. 2014;30(15):2114-20.
35. Kim D, Pertea G, Trapnell C, Pimentel H, Kelley R, Salzberg SL. TopHat2: accurate alignment of transcriptomes in the presence of insertions, deletions and gene fusions. Genome biology. 2013;14:1-13.
36. Anders S, Huber W. Differential expression analysis for sequence count data. Nature Precedings. 2010:1-.
37. Wang L, Wang S, Li W. RSeQC: quality control of RNA-seq experiments. Bioinformatics. 2012;28(16):2184-5.
38. Love MI, Huber W, Anders S. Moderated estimation of fold change and dispersion for RNA-seq data with DESeq2. Genome biology. 2014;15:1-21.
39. Kolde R. Pheatmap: pretty heatmaps. R package version. 2019;1(2):726.
40. Kevin Blighe SR, Emir Turkes, Benjamin Ostendorf, Andrea Grioni, Myles Lewis. EnhancedVolcano: Publication-ready volcano plots with enhanced colouring and labeling. R package version 1.22.0 ed2024.
41. Adrian Alexa JR. topGO: Enrichment Analysis for Gene Ontology. R package version 2.46.0 ed2024.
42. Yu G, Wang LG, Han Y, He QY. clusterProfiler: an R package for comparing biological themes among gene clusters. Omics. 2012;16(5):284-7.
43. Krämer A, Green J, Pollard J, Jr., Tugendreich S. Causal analysis approaches in Ingenuity Pathway Analysis. Bioinformatics. 2014;30(4):523-30.

44. Abdulla S, Aevermann B, Assis P, Badajoz S, Bell SM, Bezzi E, et al. CZ CELL×GENE Discover: A single-cell data platform for scalable exploration, analysis and modeling of aggregated data. bioRxiv. 2023:2023.10.30.563174.
45. Hao Y, Hao S, Andersen-Nissen E, Mauck WM, 3rd, Zheng S, Butler A, et al. Integrated analysis of multimodal single-cell data. Cell. 2021;184(13):3573-87.e29.
46. Pal B, Chen Y, Vaillant F, Capaldo BD, Joyce R, Song X, et al. A single-cell RNA expression atlas of normal, preneoplastic and tumorigenic states in the human breast. 2021;40(11):e107333.
47. Borcherding N, Vishwakarma A, Voigt AP, Bellizzi A, Kaplan J, Nepple K, et al. Mapping the immune environment in clear cell renal carcinoma by single-cell genomics. Communications Biology. 2021;4(1):122.
48. Andreatta M, Carmona SJ. UCell: Robust and scalable single-cell gene signature scoring. Computational and Structural Biotechnology Journal. 2021;19:3796-8.
49. Andrade C. Mean Difference, Standardized Mean Difference (SMD), and Their Use in Meta-Analysis: As Simple as It Gets. J Clin Psychiatry. 2020;81(5).
50. Jin S, Guerrero-Juarez CF, Zhang L, Chang I, Ramos R, Kuan C-H, et al. Inference and analysis of cell-cell communication using CellChat. Nature Communications. 2021;12(1):1088.
51. McQuin C, Goodman A, Chernyshev V, Kamentsky L, Cimini BA, Karhohs KW, et al. CellProfiler 3.0: Next-generation image processing for biology. PLoS biology. 2018;16(7):e2005970.
52. Schindelin J, Arganda-Carreras I, Frise E, Kaynig V, Longair M, Pietzsch T, et al. Fiji: an open-source platform for biological-image analysis. Nature methods. 2012;9(7):676-82.
53. Taylor-Papadimitriou J, Stampfer M, Bartek J, Lewis A, Boshell M, Lane EB, et al. Keratin expression in human mammary epithelial cells cultured from normal and malignant tissue: relation to in vivo phenotypes and influence of medium. J Cell Sci. 1989;94 (Pt 3):403-13.
54. Zarif JC, Hernandez JR, Verdone JE, Campbell SP, Drake CG, Pienta KJ. A phased strategy to differentiate human CD14+ monocytes into classically and alternatively activated macrophages and dendritic cells. Biotechniques. 2016;61(1):33-41.
55. Yamaguchi Y, Gibson J, Ou K, Lopez LS, Ng RH, Leggett N, et al. PD-L1 blockade restores CAR T cell activity through IFN-γ-regulation of CD163+ M2 macrophages. J Immunother Cancer. 2022;10(6).
56. Kadefors M, Rolandsson Enes S, Åhrman E, Michaliková B, Löfdahl A, Dellgren G, et al. CD105+CD90+CD13+ identifies a clonogenic subset of adventitial lung fibroblasts. Scientific reports. 2021;11(1):24417.
57. Piela-Smith TH, Korn JH. Aminopeptidase N: a constitutive cell-surface protein on human dermal fibroblasts. Cell Immunol. 1995;162(1):42-8.
58. Man X-Y, Finnson KW, Baron M, Philip A. CD109, a TGF-β co-receptor, attenuates extracellular matrix production in scleroderma skin fibroblasts. Arthritis Research & Therapy. 2012;14(3):R144.
59. Gao Z, Sasaoka T, Fujimori T, Oya T, Ishii Y, Sabit H, et al. Deletion of the PDGFR-β Gene Affects Key Fibroblast Functions Important for Wound Healing *. Journal of Biological

Chemistry. 2005;280(10):9375-89.
60. Lendahl U, Muhl L, Betsholtz C. Identification, discrimination and heterogeneity of fibroblasts. Nature Communications. 2022;13(1):3409.
61. Dominici M, Le Blanc K, Mueller I, Slaper-Cortenbach I, Marini FC, Krause DS, et al. Minimal criteria for defining multipotent mesenchymal stromal cells. The International Society for Cellular Therapy position statement. Cytotherapy. 2006;8(4):315-7.
62. Melissari MT, Henriques A, Tzaferis C, Prados A, Sarris ME, Chalkidi N, et al. Col6a1(+)/CD201(+) mesenchymal cells regulate intestinal morphogenesis and homeostasis. Cell Mol Life Sci. 2021;79(1):1.
63. Brinkhof B, Zhang B, Cui Z, Ye H, Wang H. ALCAM (CD166) as a gene expression marker for human mesenchymal stromal cell characterisation. Gene X. 2020;5:100031.
64. Friedman G, Levi-Galibov O, David E, Bornstein C, Giladi A, Dadiani M, et al. Cancer-associated fibroblast compositions change with breast cancer progression linking the ratio of S100A4(+) and PDPN(+) CAFs to clinical outcome. Nat Cancer. 2020;1(7):692-708.
65. Kato M, Placencio-Hickok VR, Madhav A, Haldar S, Tripathi M, Billet S, et al. Heterogeneous cancer-associated fibroblast population potentiates neuroendocrine differentiation and castrate resistance in a CD105-dependent manner. Oncogene. 2019;38(5):716-30.
66. Hutton C, Heider F, Blanco-Gomez A, Banyard A, Kononov A, Zhang X, et al. Single-cell analysis defines a pancreatic fibroblast lineage that supports anti-tumor immunity. Cancer cell. 2021.
67. Wang QA, Song A, Chen W, Schwalie PC, Zhang F, Vishvanath L, et al. Reversible De-differentiation of Mature White Adipocytes into Preadipocyte-like Precursors during Lactation. Cell metabolism. 2018;28(2):282-8.e3.
68. Cawthorn WP, Scheller EL, MacDougald OA. Adipose tissue stem cells meet preadipocyte commitment: going back to the future[S]. Journal of lipid research. 2012;53(2):227-46.
69. Jimenez MA, Akerblad P, Sigvardsson M, Rosen ED. Critical role for Ebf1 and Ebf2 in the adipogenic transcriptional cascade. Molecular and cellular biology. 2007;27(2):743-57.
70. Miyazaki T, Kitagawa Y, Toriyama K, Kobori M, Torii S. Isolation of two human fibroblastic cell populations with multiple but distinct potential of mesenchymal differentiation by ceiling culture of mature fat cells from subcutaneous adipose tissue. Differentiation. 2005;73(2-3):69-78.
71. Lejour M. Evaluation of Fat in Breast Tissue Removed by Vertical Mammaplasty. Plastic and Reconstructive Surgery. 1997;99(2):386-93.
72. Prechtel K. [Age-dependent structural changes in the female mammary gland (Area percentage determinations)]. Verh Dtsch Ges Pathol. 1970;54:393-7.
73. Pakshir P, Noskovicova N, Lodyga M, Son DO, Schuster R, Goodwin A, et al. The myofibroblast at a glance. Journal of Cell Science. 2020;133(13).
74. Hinz S, Manousopoulou A, Miyano M, Sayaman RW, Aguilera KY, Todhunter ME, et al. Deep proteome profiling of human mammary epithelia at lineage and age resolution. iScience. 2021;24(9):103026.

75. Koussounadis A, Langdon SP, Um IH, Harrison DJ, Smith VA. Relationship between differentially expressed mRNA and mRNA-protein correlations in a xenograft model system. Scientific reports. 2015;5(1):10775.
76. Nee K, Ma D, Nguyen QH, Pein M, Pervolarakis N, Insua-Rodríguez J, et al. Preneoplastic stromal cells promote BRCA1-mediated breast tumorigenesis. Nature genetics. 2023.
77. Miyako S, Koma Y-i, Nakanishi T, Tsukamoto S, Yamanaka K, Ishihara N, et al. Periostin in Cancer-Associated Fibroblasts Promotes Esophageal Squamous Cell Carcinoma Progression by Enhancing Cancer and Stromal Cell Migration. The American Journal of Pathology. 2024;194(5):828-48.
78. Lin SC, Liao YC, Chen PM, Yang YY, Wang YH, Tung SL, et al. Periostin promotes ovarian cancer metastasis by enhancing M2 macrophages and cancer-associated fibroblasts via integrin-mediated NF-κB and TGF-β2 signaling. J Biomed Sci. 2022;29(1):109.
79. Chu HY, Chen Z, Wang L, Zhang ZK, Tan X, Liu S, et al. Dickkopf-1: A Promising Target for Cancer Immunotherapy. Front Immunol. 2021;12:658097.
80. Archer M, Bernhardt SM, Hodson LJ, Woolford L, Van der Hoek M, Dasari P, et al. CCL2-Mediated Stromal Interactions Drive Macrophage Polarization to Increase Breast Tumorigenesis. International Journal of Molecular Sciences. 2023;24(8):7385.
81. Park YW, Kang YM, Butterfield J, Detmar M, Goronzy JJ, Weyand CM. Thrombospondin 2 functions as an endogenous regulator of angiogenesis and inflammation in rheumatoid arthritis. Am J Pathol. 2004;165(6):2087-98.
82. Li Q, Fu X, Yuan J, Han S. Contribution of Thrombospondin-1 and -2 to Lipopolysaccharide-Induced Acute Respiratory Distress Syndrome. Mediators Inflamm. 2021;2021:8876484.
83. Li T, Forbes ME, Fuller GN, Li J, Yang X, Zhang W. IGFBP2: integrative hub of developmental and oncogenic signaling network. Oncogene. 2020;39(11):2243-57.
84. Zhang X, Sun X, Guo C, Li J, Liang G. Cancer-associated fibroblast-associated gene IGFBP2 promotes glioma progression through induction of M2 macrophage polarization. American Journal of Physiology-Cell Physiology. 2024;326(1):C252-C68.
85. Li D, Xia L, Huang P, Wang Z, Guo Q, Huang C, et al. Cancer-associated fibroblast-secreted IGFBP7 promotes gastric cancer by enhancing tumor associated macrophage infiltration via FGF2/FGFR1/PI3K/AKT axis. Cell Death Discovery. 2023;9(1):17.
86. Crawford J, Nygard K, Gan BS, O'Gorman DB. Periostin induces fibroblast proliferation and myofibroblast persistence in hypertrophic scarring. Exp Dermatol. 2015;24(2):120-6.
87. Huang S, Fu D, Wan Z, Huang Z, Li M, Li H, et al. DKK1 Ameliorates Myofibroblast Differentiation in Urethral Fibrosis in Vivo and in Vitro by Regulating the Canonical Wnt Pathway. Int J Med Sci. 2023;20(12):1631-43.
88. Kalderén C, Stadler C, Forsgren M, Kvastad L, Johansson E, Sydow-Bäckman M, et al. CCL2 mediates anti-fibrotic effects in human fibroblasts independently of CCR2. Int Immunopharmacol. 2014;20(1):66-73.

89. Tanaka T, Narazaki M, Kishimoto T. IL-6 in inflammation, immunity, and disease. Cold Spring Harbor perspectives in biology. 2014;6(10):a016295.
90. Hu J, Zhao Q, Kong LY, Wang J, Yan J, Xia X, et al. Regulation of tumor immune suppression and cancer cell survival by CXCL1/2 elevation in glioblastoma multiforme. Sci Adv. 2021;7(5).
91. Ray A, Hu KH, Kersten K, Courau T, Kuhn NF, Zaleta-Linares I, et al. Critical role of CD206+ macrophages in promoting a cDC1-NK-CD8 T cell anti-tumor immune axis. bioRxiv. 2024.
92. Wu J, Liu X, Wu J, Lou C, Zhang Q, Chen H, et al. CXCL12 derived from CD248-expressing cancer-associated fibroblasts mediates M2-polarized macrophages to promote nonsmall cell lung cancer progression. Biochim Biophys Acta Mol Basis Dis. 2022;1868(11):166521.
93. Li X, Bu W, Meng L, Liu X, Wang S, Jiang L, et al. CXCL12/CXCR4 pathway orchestrates CSC-like properties by CAF recruited tumor associated macrophage in OSCC. Experimental cell research. 2019;378(2):131-8.
94. Faas M, Ipseiz N, Ackermann J, Culemann S, Grüneboom A, Schröder F, et al. IL-33-induced metabolic reprogramming controls the differentiation of alternatively activated macrophages and the resolution of inflammation. Immunity. 2021;54(11):2531-46.e5.
95. Furukawa S, Moriyama M, Miyake K, Nakashima H, Tanaka A, Maehara T, et al. Interleukin-33 produced by M2 macrophages and other immune cells contributes to Th2 immune reaction of IgG4-related disease. Scientific reports. 2017;7(1):42413.
96. Xiao P, Wan X, Cui B, Liu Y, Qiu C, Rong J, et al. Interleukin 33 in tumor microenvironment is crucial for the accumulation and function of myeloid-derived suppressor cells. Oncoimmunology. 2016;5(1):e1063772.
97. Sami E, Paul BT, Koziol JA, ElShamy WM. The Immunosuppressive Microenvironment in BRCA1-IRIS–Overexpressing TNBC Tumors Is Induced by Bidirectional Interaction with Tumor-Associated Macrophages. Cancer research. 2020;80(5):1102-17.
98. Molgora M, Esaulova E, Vermi W, Hou J, Chen Y, Luo J, et al. TREM2 Modulation Remodels the Tumor Myeloid Landscape Enhancing Anti-PD-1 Immunotherapy. Cell. 2020;182(4):886-900.e17.
99. Shalabi SF, Miyano M, Sayaman RW, Lopez JC, Jokela TA, Todhunter ME, et al. Evidence for accelerated aging in mammary epithelia of women carrying germline BRCA1 or BRCA2 mutations. Nature Aging. 2021;1(9):838-49.
100. Miyano M, Sayaman RW, Shalabi SF, Senapati P, Lopez JC, Angarola BL, et al. Breast-Specific Molecular Clocks Comprised of ELF5 Expression and Promoter Methylation Identify Individuals Susceptible to Cancer Initiation. 2021;14(8):779-94.
101. Ogony J, Hoskin TL, Stallings-Mann M, Winham S, Brahmbhatt R, Arshad MA, et al. Immune cells are increased in normal breast tissues of BRCA1/2 mutation carriers. Breast Cancer Res Treat. 2023;197(2):277-85.
102. van Vugt MATM, Parkes EE. When breaks get hot: inflammatory signaling in BRCA1/2-mutant cancers. Trends in Cancer. 2022;8(3):174-89.

103. Li Y, Dong W, Zhang P, Zhang T, Ma L, Qu M, et al. Comprehensive Analysis of Regulatory Factors and Immune-Associated Patterns to Decipher Common and BRCA1/2 Mutation-Type-Specific Critical Regulation in Breast Cancer. Frontiers in cell and developmental biology. 2021;9.
104. Wen WX, Leong C-O. Association of BRCA1- and BRCA2-deficiency with mutation burden, expression of PD-L1/PD-1, immune infiltrates, and T cell-inflamed signature in breast cancer. PloS one. 2019;14(4):e0215381.
105. Paauwe M, Schoonderwoerd MJA, Helderman RFCP, Harryvan TJ, Groenewoud A, van Pelt GW, et al. Endoglin Expression on Cancer-Associated Fibroblasts Regulates Invasion and Stimulates Colorectal Cancer Metastasis. Clinical Cancer Research. 2018;24(24):6331-44.
106. Kumar B, Khatpe AS, Guanglong J, Batic K, Bhat-Nakshatri P, Granatir MM, et al. Stromal heterogeneity may explain increased incidence of metaplastic breast cancer in women of African descent. Nat Commun. 2023;14(1):5683.
107. Nishikoba N, Kumagai K, Kanmura S, Nakamura Y, Ono M, Eguchi H, et al. HGF-MET Signaling Shifts M1 Macrophages Toward an M2-Like Phenotype Through PI3K-Mediated Induction of Arginase-1 Expression. Front Immunol. 2020;11:2135.
108. Babazadeh S, Nassiri SM, Siavashi V, Sahlabadi M, Hajinasrollah M, Zamani-Ahmadmahmudi M. Macrophage polarization by MSC-derived CXCL12 determines tumor growth. Cell Mol Biol Lett. 2021;26(1):30.
109. Mehta AK, Kadel S, Townsend MG, Oliwa M, Guerriero JL. Macrophage Biology and Mechanisms of Immune Suppression in Breast Cancer. Front Immunol. 2021;12:643771.
110. Posadas EM, Swami U, Dorff TB, Tighiouart M, Wang JJ, Zhu Y, et al. A randomized phase II study of apalutamide with or without carotuximab (ant-CD105) in metastatic, castration-resistant prostate cancer. Journal of Clinical Oncology. 2023;41(16_suppl):TPS5107-TPS.
111. Haaland GS, Falk RS, Straume O, Lorens JB. Association of Warfarin Use With Lower Overall Cancer Incidence Among Patients Older Than 50 Years. JAMA Intern Med. 2017;177(12):1774-80.
112. Guo Q, Minnier J, Burchard J, Chiotti K, Spellman P, Schedin P. Physiologically activated mammary fibroblasts promote postpartum mammary cancer. JCI Insight. 2017;2(6).
113. Miyano M, Sayaman RW, Stoiber MH, Lin CH, Stampfer MR, Brown JB, et al. Age-related gene expression in luminal epithelial cells is driven by a microenvironment made from myoepithelial cells. Aging (Albany NY). 2017;9(10):2026-51.
114. Rosalyn WS, Masaru M, Parijat S, Arrianna Z, Sundus S, Michael ET, et al. Luminal epithelial cells integrate variable responses to aging into stereotypical changes that underlie breast cancer susceptibility. bioRxiv. 2022:2022.09.22.509091.
115. Longacre TA, Bartow SA. A correlative morphologic study of human breast and endometrium in the menstrual cycle. Am J Surg Pathol. 1986;10(6):382-93.
116. Fanger H, Ree HJ. Cyclic changes of human mammary gland epithelium in relation to the menstrual cycle—an ultrastructural study. Cancer. 1974;34(3):574-85.

Figures

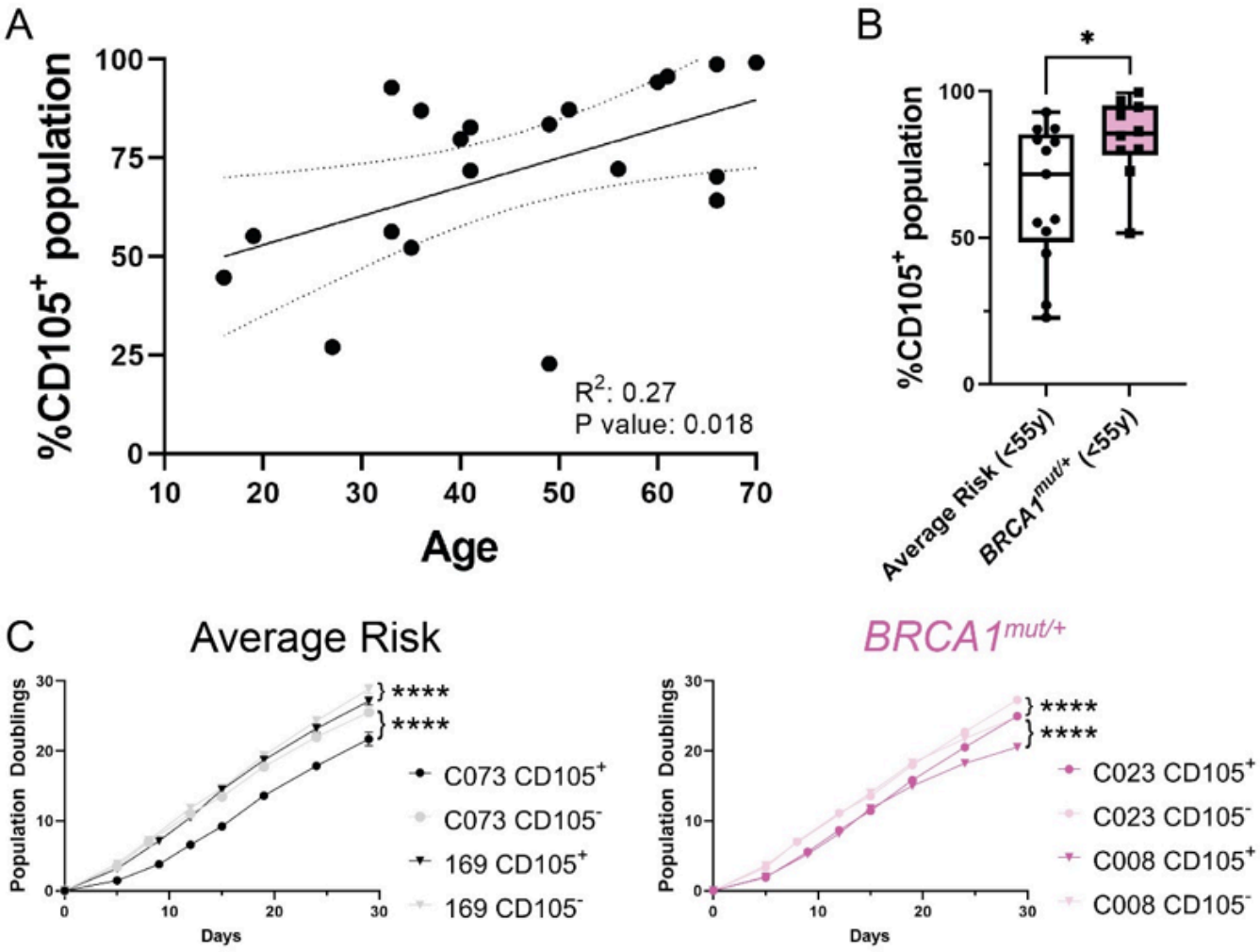

Figure 1

CD105^{+} fibroblasts are more abundant in cultures from older women and women with *BRCA1* mutations. **A** Flow cytometry measurement of CD105 proportion in fibroblasts from women ranging from 16 to 70 years of age (n=20); simple linear regression plotted with 95% confidence intervals. **B** Flow cytometry measurement of CD105 proportion in fibroblasts from age-matched women with varying *BRCA1* mutational status (AR n=13, *BRCA1*$^{mut/+}$ n=10); unpaired t test with Welch's correction (P value = 0.0263). **C** Population doublings of CD105^{-} & CD105^{+} fibroblasts from women with different *BRCA1* mutational status in serial passage subculture, error bars represent standard deviation, two-way ANOVA (**** = P < 0.0001).

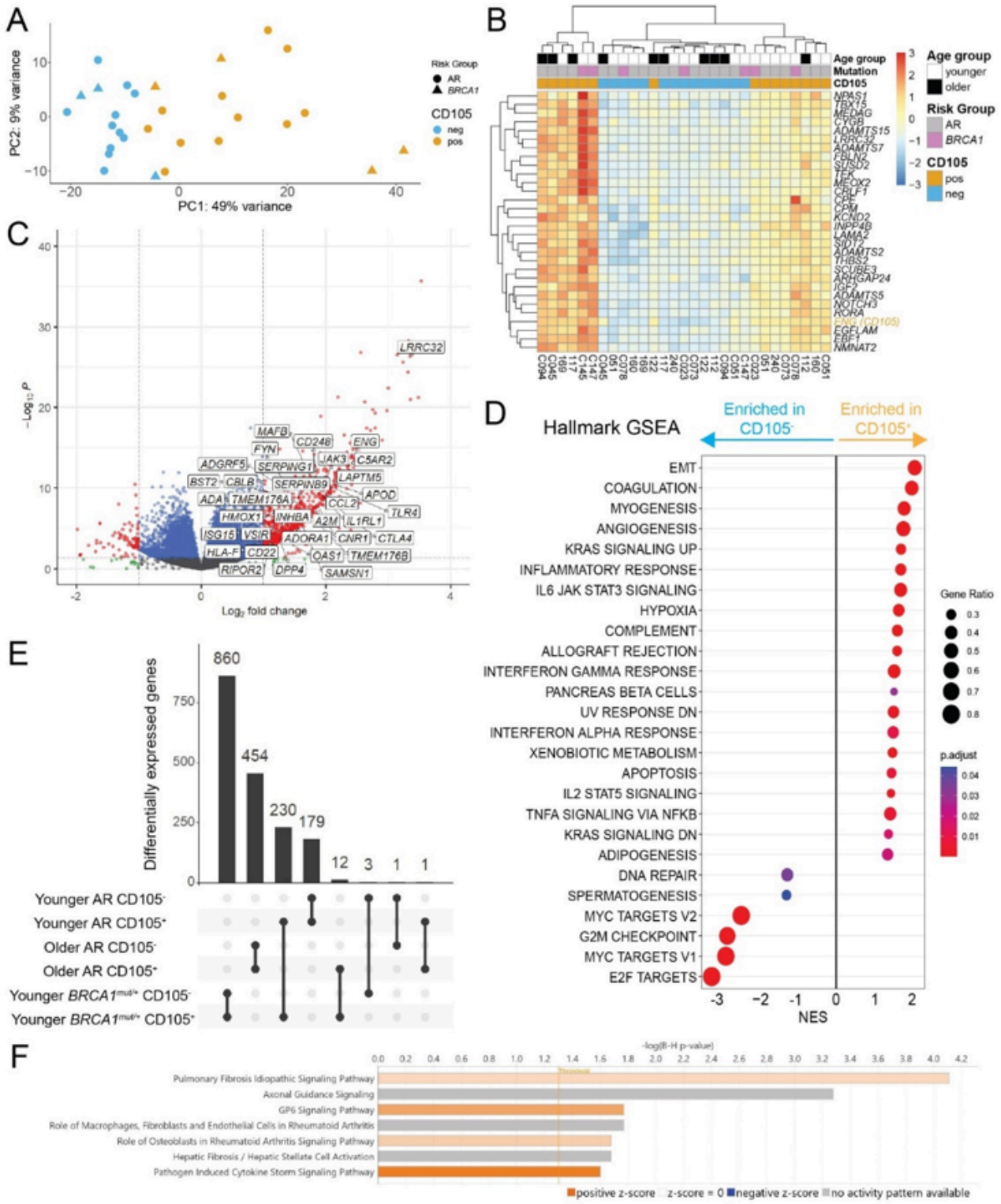

Figure 2

CD105^{+} fibroblasts are enriched for adipogenesis, angiogenesis, and negative regulation of the immune system pathways. **A** Principal component analysis (PCA) of all expressed genes for the 29 samples analyzed by RNA-seq **B** Heatmap of samples (columns) clustered based on expression of top 30 differentially expressed genes (rows) between CD105^{+} & CD105^{-} fibroblasts; values centered and scaled

by row. **C** Volcano plot of differentially expressed genes in CD105^{+} compared with CD105^{-} fibroblasts with significantly upregulated genes related to the GO term “negative regulation of immune system” labeled along with *ENG (CD105*) and *CD248*. **D** MSigDB hallmark pathways enriched in CD105^{-} & CD105^{+} fibroblasts. **E** Number of differentially expressed genes between fibroblasts from each group. **F** Ingenuity pathway analysis of differentially expressed genes between *BRCA1*$^{mut/+}$ CD105^{+} & younger AR CD105^{+} fibroblasts. Data were analyzed with the use of QIAGEN IPA (QIAGEN Inc., https://digitalinsights.qiagen.com/IPA).

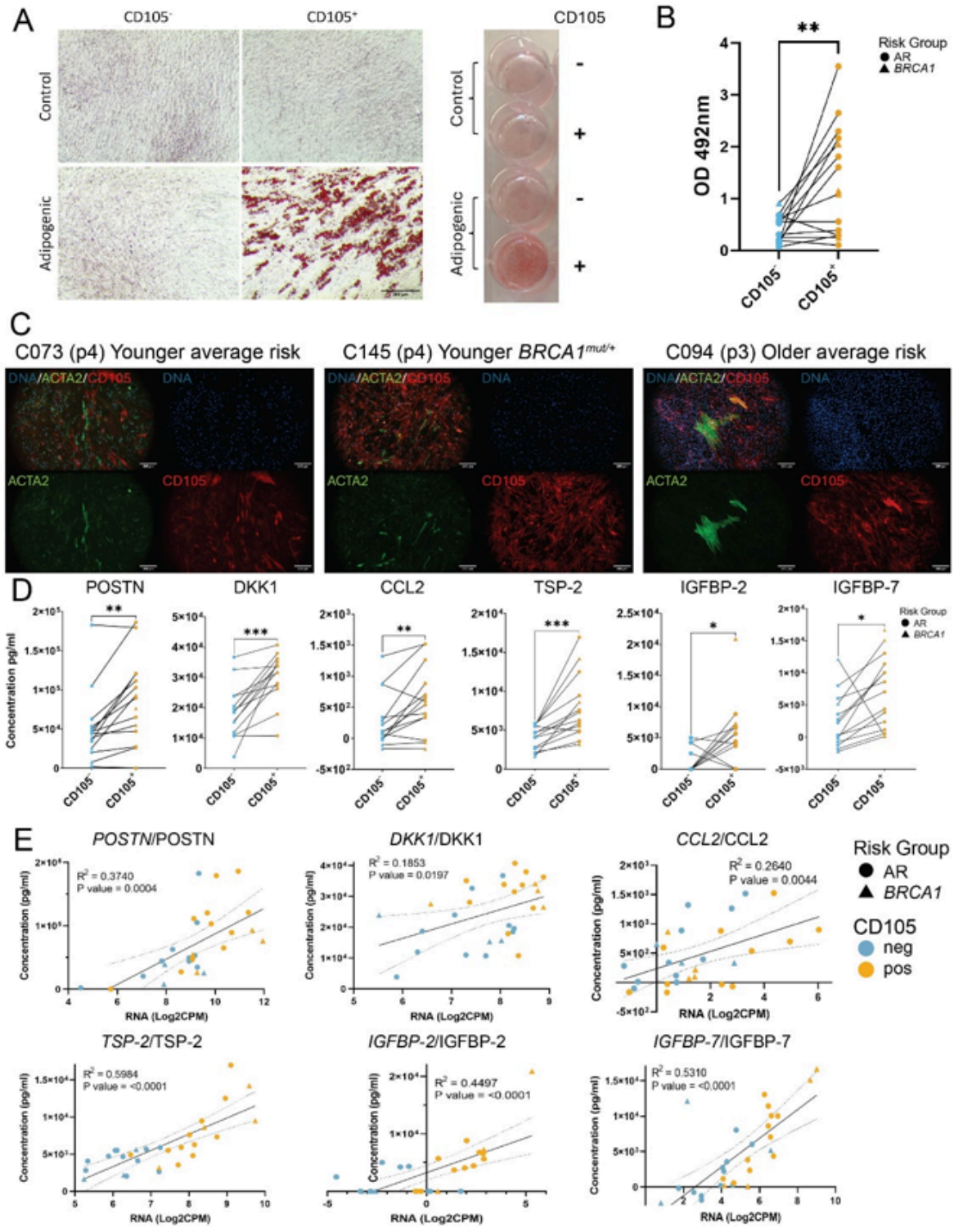

Figure 3

$CD105^+$ fibroblasts exhibit robust adipogenesis and secrete proteins related to polarization of macrophages and angiogenesis. **A** (left panel) Representative brightfield images (10X objective) from CD105 sorted fibroblasts from strain 169 grown in control or adipogenic media for 2 weeks, fixed, and neutral lipids stained with oil red O (ORO) (scale bar = 200 μm). (right panel) Photograph of wells of a 12-well plate imaged in left panel. **B** Quantification of ORO staining in sorted fibroblasts grown in adipogenic media by measuring OD (optical density) 492nm using a plate-reader spectrophotometer, paired t test (P value = 0.0063). **C** Representative fluorescent images of DNA (Hoechst blue), ACTA2 (green), and CD105 (red) expression in fibroblasts from 3 different donors (scale bar = 200 μm). **D** Concentration of each analyte measured in supernatant of sorted $CD105^+$ and $CD105^-$ fibroblasts cultured for 4 days, Paired t test. **E** Correlation between protein and transcript level expression of each analyte in each strain, ($CD105^-$ fibroblasts in blue and $CD105^+$ fibroblasts in orange) simple linear regression plotted with 95% confidence intervals.

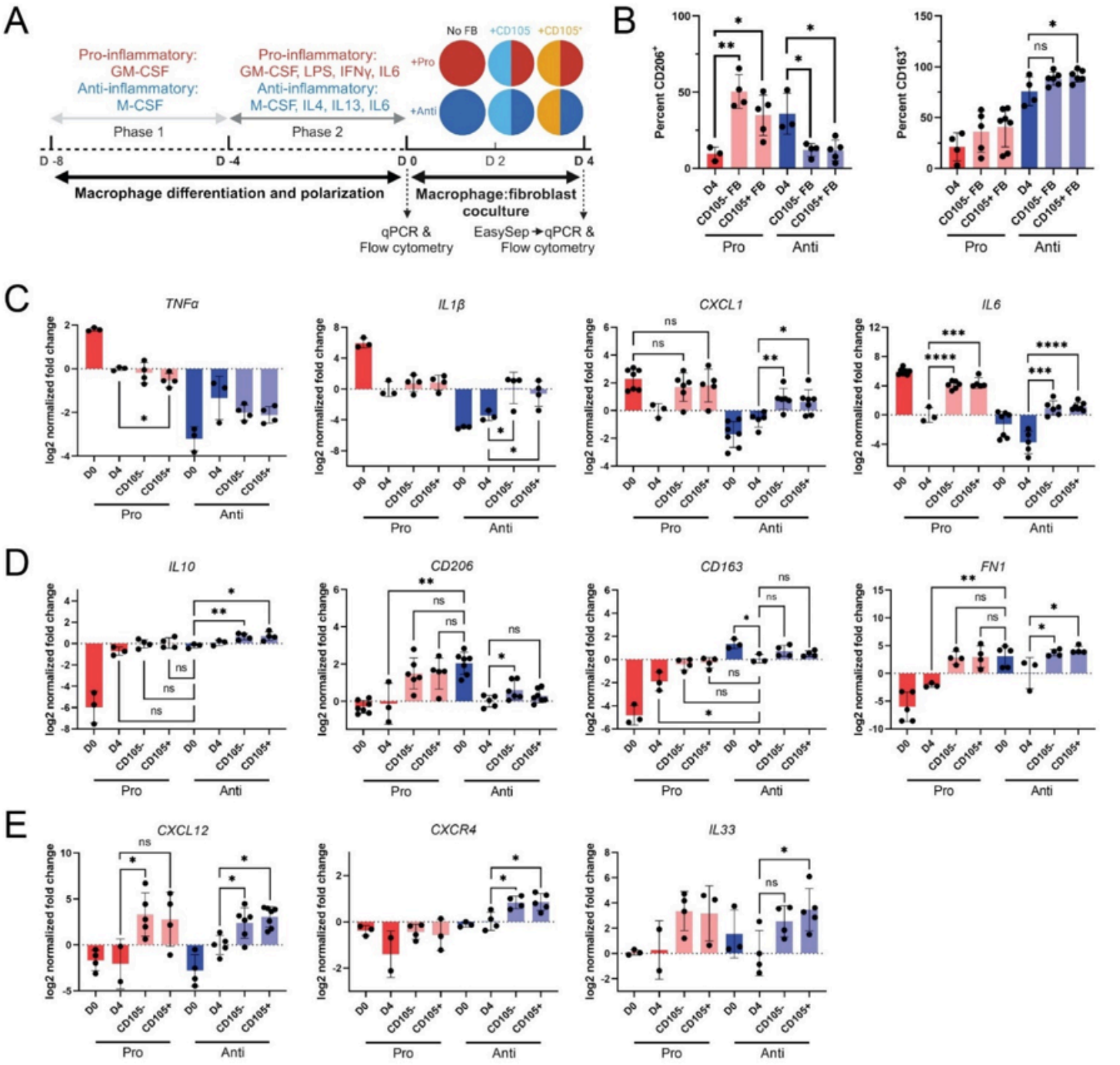

Figure 4

Fibroblasts influence macrophage polarization. **A** Scheme for macrophage polarization and subsequent fibroblast coculture. **B** Flow cytometry analysis of macrophages enriched for CD45 expression following 4 days of culture without polarization media. **C-E** qPCR analysis of macrophages enriched for CD45 expression following 4 days of culture without polarization media. **C** Pro-inflammatory genes normalized to D4 pro-inflammatory macrophages in monoculture. **D** Anti-inflammatory genes normalized to D4 anti-inflammatory macrophages in monoculture. **E** Tumor-associated macrophage genes normalized to D4 anti-inflammatory macrophages in monoculture, unpaired t tests used to determine significance (ns $P > 0.05$, * $P \leq 0.05$, ** $P \leq 0.01$, *** $P \leq 0.001$, **** $P \leq 0.0001$) and error bars represent standard deviation.

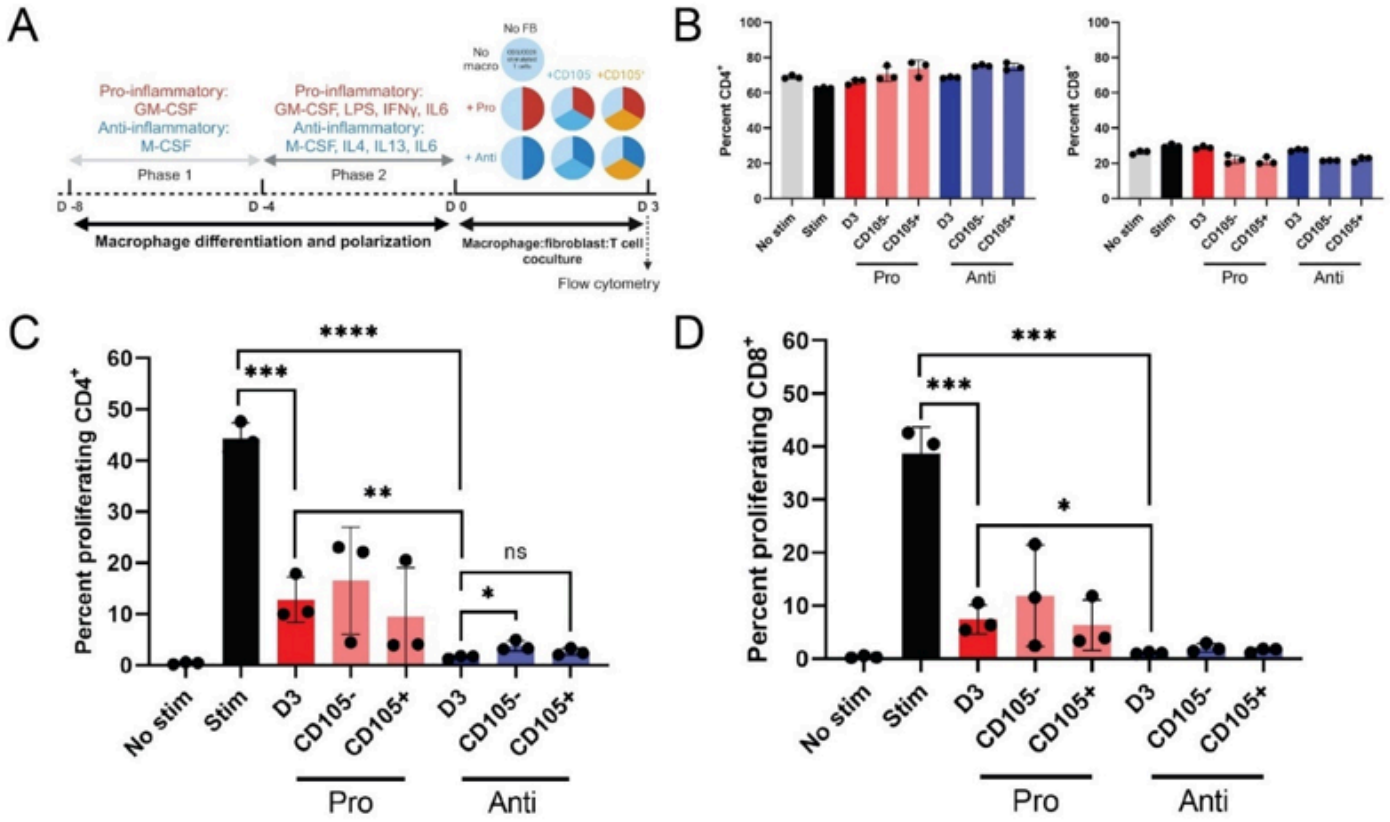

Figure 5

Fibroblasts have a modest impact on macrophages' ability to inhibit T cell proliferation. **A** Scheme for macrophage polarization and subsequent fibroblast and T cell coculture. **B** T cell subtype composition after 3 days in various coculture conditions: (left panel) percentage $CD3^+CD4^+$ T cells (right panel) percentage $CD3^+CD8^+$ T cells. **C&D** CellTrace was used to label T cells and measure proliferation of T cell subsets after 3 days in various coculture conditions. **C** Percentage proliferating $CD3^+CD4^+$ T cells. **D** Percentage proliferating $CD3^+CD8^+$ T cells, GraphPad Prism v.9.3.1 was used to perform two-tailed unpaired T-tests and error bars represent standard deviation.

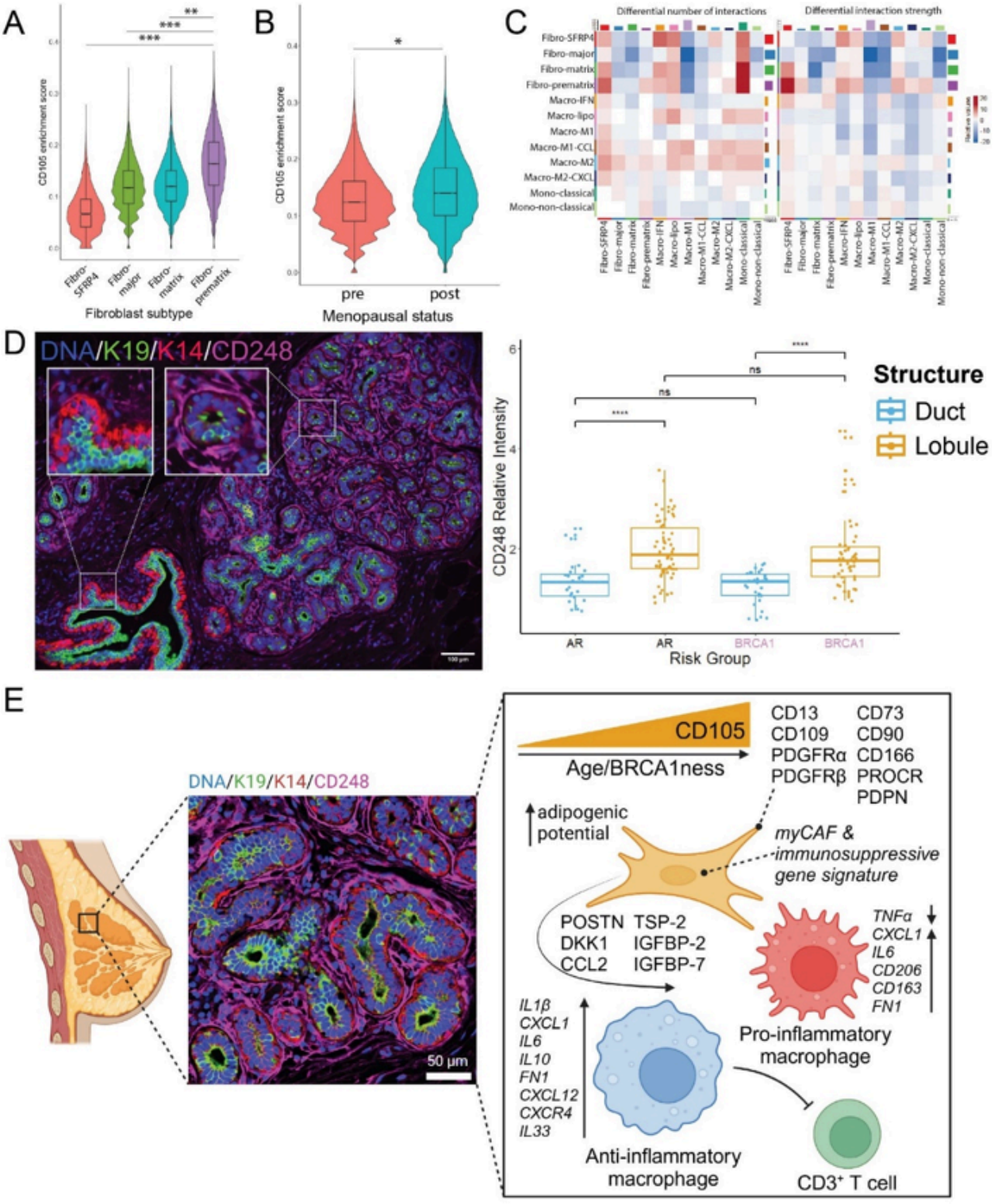

Figure 6

Contextualizing the CD105^{+} signature. **A&B** scGSEA was performed on fibroblasts from a scRNA-seq dataset (Kumar et al. 2023) using a custom gene list comprised of the top 30 gene differentially expressed in CD105^{+} fibroblasts (**Figure 2B)**; standardized mean difference: small effect size (0.2 – 0.5) *, medium effect size (0.5 – 0.8) **, large effect size (>0.8) ***. **A** Split by fibroblast subtype. **B** Fibroblasts split by menopausal status. **C** CellChat was used to infer number and strength of interactions

between different cell subtypes from pre and postmenopausal women (Kumar et al. 2023). **D** (left panel) Representative fluorescent image (20X objective) of DNA (Hoechst blue), KRT19 (K19 green), KRT14 (K14 red), and CD248 (magenta) in a tissue section from donor C073 (scale bar = 100 μm). (right panel) Quantification of CD248 expression in different structures in tissue sections from donors with different *BRCA1* mutational backgrounds, (AR duct n = 28, AR lobule n = 66, HR duct = 30, HR lobule = 52) Mann-Whitney U test (**** = < 0.0001, ns = > 0.05). **E** Graphical summary of $CD105^{+}$ fibroblasts.

Supplementary Files

This is a list of supplementary files associated with this preprint. Click to download.

- supplementaryfigures.pdf
- supplementaryinformationtablesfinalrevisions.xlsx